Hydration, mechanical and transfer properties of blended cement pastes and mortars prepared with recycled powder or limestone filler

Mahmoud Nacer-Eddine Hamdadou, François Bignonnet, Walid Deboucha, Harifidy Ranaivomanana, Nordine Leklou, Karima Arroudj

Hydration, mechanical and transfer properties of blended cement pastes and mortars prepared with recycled powder or limestone filler

Mahmoud Nacer-eddine HAMDADOU [a, b,*], François BIGNONNET [a], Walid DEBOUCHA [c], Harifidy RANAIVOMANANA [a], Nordine LEKLOU [a], Karima ARROUDJ [b]

a Nantes Université, École Centrale Nantes, CNRS, GeM, UMR 6183, F-44600 Saint-Nazaire, France

b Building in Environment Laboratory, Faculty of Civil Engineering, University of Sciences and Technology Houari Boumediene, P.O. Box 32, El Alia-Bab Ezzouar, Alger, Algeria

c CESI LINEACT, 80 Rue Edmund Halley, Rouen Madrillet Innovation, F-76808 Saint-Étienne-du-Rouvray, France

* Corresponding author. mahmoud-nacer-eddine.hamdadou@univ-nantes.fr

Abstract

The fine fraction (< 80 µm) of recycled aggregates from construction and demolition wastes, currently considered as waste, is investigated as a candidate mineral additive for partial replacement of Ordinary Portland Cement (OPC) to reduce the environmental impact of cementitious materials. Although recycled powder could affect hydration reactions due to the presence of residual anhydrous cement particles and to its high specific surface area, very few studies are available in literature concerning these aspects. Cement pastes and mortars prepared with 0%, 10%, and 20% replacement by weight of OPC by either Recycled Powder (RP) or Limestone Filler (LF) are compared in terms of hydration degree, mechanical and transport properties using several techniques, including Isothermal Calorimetry (IC), Thermogravimetric Analysis (TGA), water porosity, mercury intrusion porosimetry and gas permeability. The results revealed that mixtures blended with RP or LF have a similar decrease in the overall hydration degree compared to the hydration degree of pure OPC mixture due to a dilution effect, although both additives have a small reactivity. A moderate increase in porosity and intrinsic permeability with the replacement rate is observed. Pastes and mortars blended with RP have a compressive strength and a Young modulus nearly identical to those with the same amount of LF, despite RP having worse properties than LF. A multiscale micromechanical model is established and reproduces faithfully these experimental results for the elastic moduli, based on the simplified assumptions that LF is nearly inert while RP reduces the effective water to binder ratio by both absorption of water and internal hydration reactions.

Keywords: Recycled powder; Limestone filler; Degree of hydration; Mechanical properties; Multiscale model

1. Introduction

The use of recycled aggregates obtained from construction and demolition wastes considerably increases in the concrete industry in order to reduce consumption and to preserve natural resources for future generations [1], [2]. Several works have been carried out on the incorporation of recycled aggregates in the granular skeleton of concrete in order to study their influence on the mechanical properties, microstructure and durability performance of concrete [3],[4],[5]. The valorization of demolition wastes through partial replacement of natural coarse aggregates in concrete has been defined by standards that limit the rate of replacement depending on the construction sites. Among them, the European Standard

NF EN 206/ CN [6] authorizes a quantity of recycled concrete aggregates which concerns gravel and sand only. The use of these aggregates depends on the nature of the aggressive environment.

The annual global production of cement, which is the main compound of concrete formulations, is responsible for at least 5 % of global CO_2 emissions [7], [8]. In fact, the production of 1 ton of Portland cement releases the equivalent of 0.7 ton of CO_2 [9]. Among the existing solution to mitigate this problem, one can mention the partial replacement of cement by mineral additives, natural or industrial co-products (limestone filler, natural pozzolan, slag, fly ashes, …etc.) [10],[11],[12]. Physical, filler and/or chemical effects may be involved between cement and mineral additive. Regarding physical effects, the presence of additional fine particles improves the compactness of concrete, simultaneously, an increase the binder's porosity can be observed due to the dilution effect [13]. The filler effect is defined as the ability of mineral additives to improve the hydration reaction through heterogeneous nucleation and dilution effects. Meanwhile, the chemical effects, which consist of hydraulic or pozzolanic reaction, lead to form more hydration products and thus, improve concrete properties [14],[15]. For the same objective, several authors investigated the addition of recycled powder in cement Portland [16],[17].

Recycled Powder (RP), produced from construction and demolition wastes, contains some particles of old concrete or masonry and other type of materials like gypsum, ceramic, wood, glass and brick. After the crushing of construction and demolition waste, the fraction of particles whose size is below 150 µm is about 20% [16]. Due to current normative limitations [6], this fine fraction is not valorized. The use of RP as a partial replacement of Portland cement to produce recycled cement paste opens up new prospects in the exploitation of construction and demolition wastes, which can reduce environmental pollution by reducing CO_2 emissions from clinker production [16]. The RP contains siliceous oxide and calcareous oxide, and some hydrated and non-hydrated components of the old cement paste [16]. The RP are rarely used in constructions due to their high porosity and water absorption [18]. The carbonation treatment appeared as a solution to enhance the density of RP though reduction of its porosity and water absorption [19], [20]. Previous studies have shown that replacing cement with RP influences the workability of mixtures where the fluidity decreases with increasing the rate replacement level [21], [22], [23]. Most of the previous studies on the effect of RP were dedicated to investigations on their effect on physical and mechanical properties of concretes (workability, strength, etc.).

However, further research on the chemical properties (e.g. hydration kinetics) of RP blended cementitious materials, as well as on their transfer properties (e.g. porosity, permeability), is needed to provide a better understanding of the effect of cement replacement by RP. Hence in this work, the influence of cement replacement by untreated recycled powder, on the hydration evolution of cement paste formulations, as well as on the mechanical and transfer properties evolutions of different mortars formulations is investigated. The investigation features a comparison of performances of cements pastes and mortars prepared with recycled powder to those obtained for mixtures incorporating limestone filler with the same replacement levels (10% and 20%). To identify the main mechanisms responsible for the obtained properties, the investigation combines a thorough experimental characterization of the cements pastes and mortars with a multiscale micromechanical and hydration model.

The article is organized as follows: Materials and testing methods are presented in section 2. A multi-scale micromechanical model is presented in section 3 to estimate the variation of the dynamic Young modulus during hydration of cement pastes and mortars, accounting for the nature and replacement level of the two types of mineral additives used. Section 4 presents the findings from both experimental and modeling studies on the effect of partial replacement of cement by RP on cement paste and mortar properties. These results are compared to reference mixtures that either have no replacement or are replaced with LF. subsection 4.1, the hydration heat from isothermal calorimetry test and the hydration degree estimated from thermogravimetric analysis (TGA) using the methodology suggested by Deboucha et al. [24] are presented and comparatively discussed. Second in subsection 4.2, water porosity, mercury intrusion porosimetry and gas permeability results are discussed. Finally, compressive strength and dynamic Young's modulus obtained experimentally are presented in subsection 4.3. To further

explain the findings obtained, the latter are compared to modeled stiffness for both cement pastes and mortars as a function of the degree of hydration determined by the method based on TGA.

2. Materials and Method

2.1. Materials

2.1.1. Cement and Sand

The Ordinary Portland Cement (OPC) used in this study is a CEM I 52.5N CE CP2 NF from Saint-Pierre la Cour (France), in accordance with European standard [NF EN 197-1] [25]. It has a density of 3120 kg/m^3 and a specific surface area of 930 m^2/kg obtained from BET measurements. Its chemical composition and physical characteristics are detailed in Table 1. Its Bogue's composition was 63% C_3S, 13.5% C_2S, 9.6%, 9.6% C_3A and 9% C_4AF. The sand used for the formulation of mortars is a standardized siliceous sand of Leucate (France), [NF EN 196-1][26]. The particle size of sand ranges from 0 to 2 mm, its density is 2600 kg/m^3.

2.1.2. Recycled Powder (RP) and Limestone Filler (LF)

The Recycled Powder (RP) is processed out of recycled aggregates from an industrial recycling platform for concrete and demolition waste (Quimper, France). The recycled aggregates have been received in a 1m^3 batch containing mixed fines, sand and gravels. This mix contains about 15% of fines below 80 µm. To produce all the formulations or pastes and mortars investigated in this paper and other ongoing studies, sieving of three such batches would have been required. Such volume can be sieved in an industrial facility but not in our laboratory. Hence, the RP used in this study comes from two processes. The first part comes from direct sieving at 80µm the received material. The second part was obtained by artificially crushing part of the 8-20mm recycled gravels. Crushing has been carried out with a jaw crusher with an 80 x 50 mm entry. The jaw crusher produced 0-5mm particles, which have been sieved to produce <80µm RP. Powders coming from both processes have then been dry-mixed to produce a single batch. The density of this RP is 2300 kg/m^3. The BET analysis provides a specific surface area of 6377 m^2/kg.

The Limestone Filler (LF) used is a BETOCARB HP (Erbray, France). Its $CaCO_3$ content is 97.5%. It has a specific surface area of 382 m^2/kg deduced from BET measurements, and an absolute density of 2710 kg/m^3. The chemical composition and physical characteristics are detailed in Table 1. The particle size distribution of RP and LF determined by laser diffraction analyzer and X-ray diffraction patterns are shown in Fig. 1 and Fig. 2 respectively.

Table 1 : Chemical composition and physical characteristics of cement and additions

	OPC	RP	LF
Chemical composition (%)			
SiO_2	21.30	50.19	1.20
Al_2O_3	5.51	10.22	/
Fe_2O_3	2.96	2.50	/
CaO	65.39	16.83	97.50
MgO	1	0.79	/
SO_3	3.10	0.86	0.01

K_2O	0.04	2.61	0.0012
Na_2O	0.01	1.04	0.0008
Physical characteristics			
Density (kg/m^3)	3120	2300	2700
BET (m^2/kg)	930	6377	382
d_{10} [µm]	0.96	0.18	1.03
d_{50} [µm]	9.58	8.05	9.32
d_{90} [µm]	32.47	47.14	35.44

The median size (50 % passing by mass) of the RP particles is 8.05 µm compared to 9.58 µm for OPC and 9.32 µm for LF. The percentage of passersby at 50 µm is 92.3% for RP compared to 99.55% for OPC and 95.5% for LF. The BET-measured fineness of recycled powder is much higher than that of limestone filler and cement. This is partly attributed to the high specific surface area of gel porosity of hydrated cement paste fragments within the RP, and to the presence of around 20% of submicron particles (see Fig. 1).

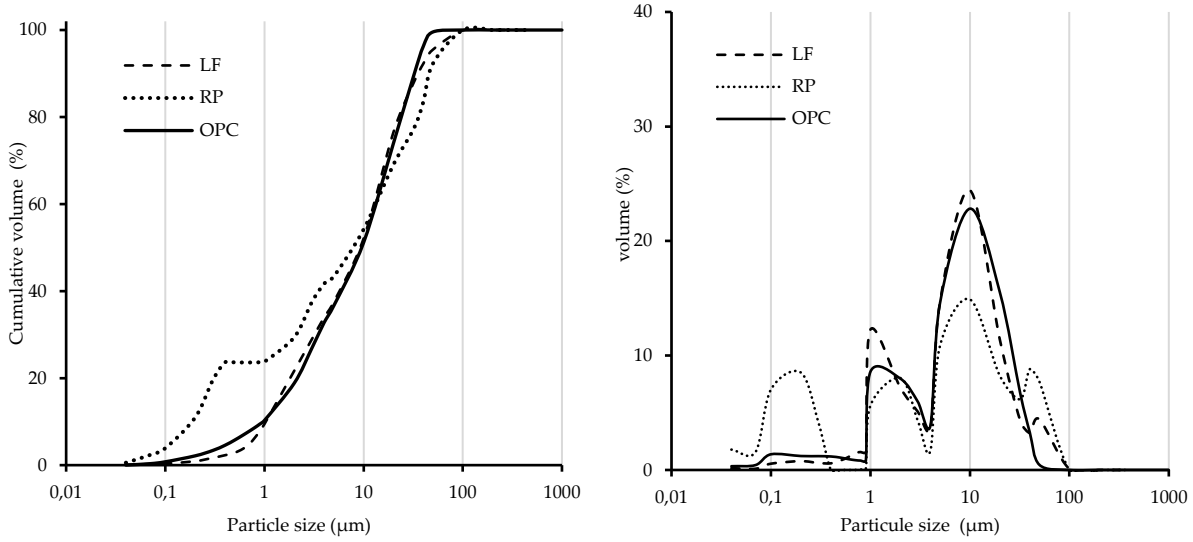

Fig. 1: Particle size distribution of cement and additions

Fig. 2 shows the results of X-Ray Diffraction (XRD) for the RP and LF. The XRD patterns for recycled powder show the presence of multiple phases. The peaks of Aluminum Oxide, Calcite, Potassium-Feldspar and Quartz were identified. Conversely for limestone filler the only one phase is Calcite. These results confirm the chemical composition for the mineral additives used in this study (Table 1).

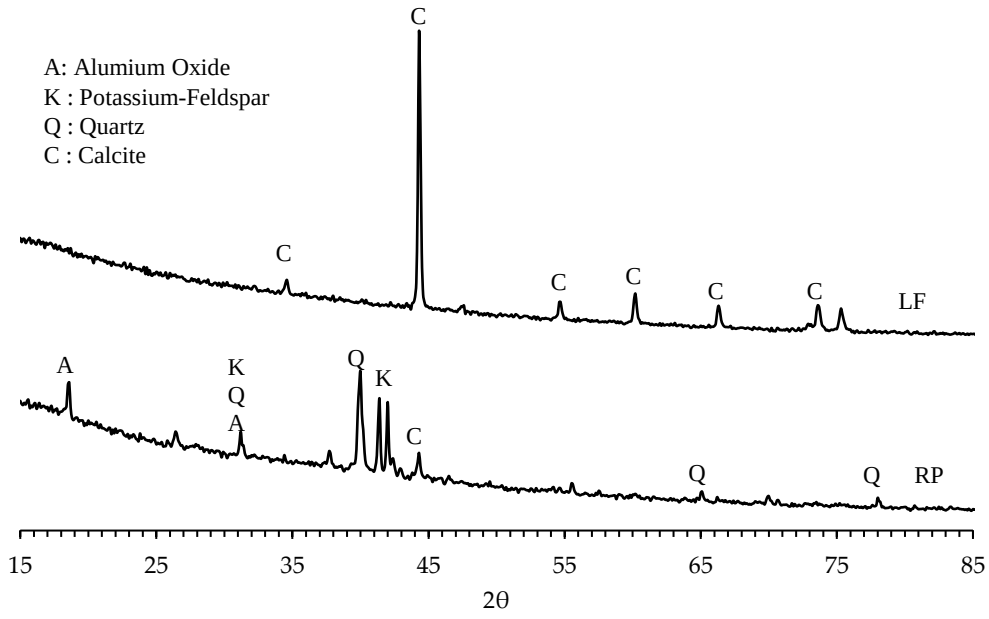

Fig. 2 : X-ray diffraction of recycled powder and limestone filler

2.2. Mixtures and methods

Different formulations of cement pastes and mortars having a nominal water to binder ratio of 0.5 are tested in the present study. Due to the difference in water adsorption of LF and RP, different effective water to binder ratio are expected. This point is quantified in the multiscale modeling sections 3.3 and 3.4. Cement paste mixtures are noted as PR, P10RP, P10LF, P20RP and P20LF while mortars are named as MR, M10RP, M10LF, M20RP and M20LF. These nomenclatures correspond to replacement levels of cement by RP and LF (0%, 10% and 20% respectively) (Table 2). A sand to binder ratio of 3 is adopted for mortar formulations. Mixtures details are provided in Table 3.

The tests performed on the cement pastes consist in isothermal calorimetry, dynamic Young modulus measurements and thermogravimetric analysis (TGA). Isothermal calorimetry allows to evaluate the heat of hydration while TGA makes it possible to estimate the degree of hydration at different ages. Prismatic 40x40x160 mm^3 specimens for dynamic modulus are formulated according to the standard NF EN 196-3[27] and are kept in water at 20 ± 2 °C for 3, 7, 28 and 90 days respectively. For TGA test, the specimens are placed in hermetically closed PVC vials which are conserved in a conditioned room at 20 ± 2 °C.

The tests performed on mortars concern the measurement of mechanical, microstructural and transport properties. The 40x40x160 mm^3 prisms have been cast for measures of compressive and flexural strength, dynamic Young modulus, water porosity and mercury intrusion porosimetry. Gaz permeability tests have also been carried out on cylinders of height 140 mm and diameter 70 mm. The mixtures are prepared according to the standard NF EN 196-1 [26]. The specimens were demolded 24h later and stored in water at 20 ± 2 °C.

Table 2 : Cement paste compositions

	PR	P10RP	P10LF	P20RP	P20LF
Cement (%)	100	90	90	80	80
RP (%)	/	10	/	20	/
LF (%)	/	/	10	/	20
W/B	0.5	0.5	0.5	0.5	0.5

Table 3 : Mortar compositions and density

	MR	M10RP	M10LF	M20RP	M20LF
Cement (g)	450	405	405	360	360
RP (g)	/	45	/	90	/
LF (g)	/	/	45	/	90
Water (g)	225	225	225	225	225
Sand (g)	1350	1350	1350	1350	1350
Binder Density (kg/m^3)	2564	2546	2555	2528	2546

2.3. Testing methods

2.3.1. Heat of hydration

The effect of replacing part of cement by either recycled powder or limestone filler on early ages hydration kinetics was evaluated by using a multi-channel isothermal calorimeter device (TAM Air) [28]. Right after mixing binders with water two samples of 4-6 g were placed into standard plastic vial and loaded into the channel of the isothermal calorimeter. Both heat and heat flow were monitored continuously for 7 days at 20°C.

2.3.2. Thermogravimetric analysis

The thermogravimetric analysis (TGA) was performed at 3, 7, 28 and 90 days respectively on powdered samples in order to estimate the degree of hydration of blended cement paste. For that purpose, samples were crushed and sieved to obtain a grain size lower than 45 µm. A Mettler Toledo TGA/DSC device was used to measure the evolution of mass versus the temperature under an N_2 environment. The temperature varies from 25 to 1050 °C at a rate of 5 °C by min.

The method used to estimate the degree of hydration is based on the decomposition of cement hydrates at three different stages and on the mass loss of water bound to the hydrates. The initial stage between 105 and 400 °C, noted as (Ldh), represents the dehydration reaction (Fig. 3). The second stage noted as (Ldx) corresponds to the dehydroxylation of portlandite between 400 and 600 °C. Finally, the last stage between 600 and 800 °C noted as (Ldc) is related to the decarbonation of calcium carbonate $CaCO_3$ [24].

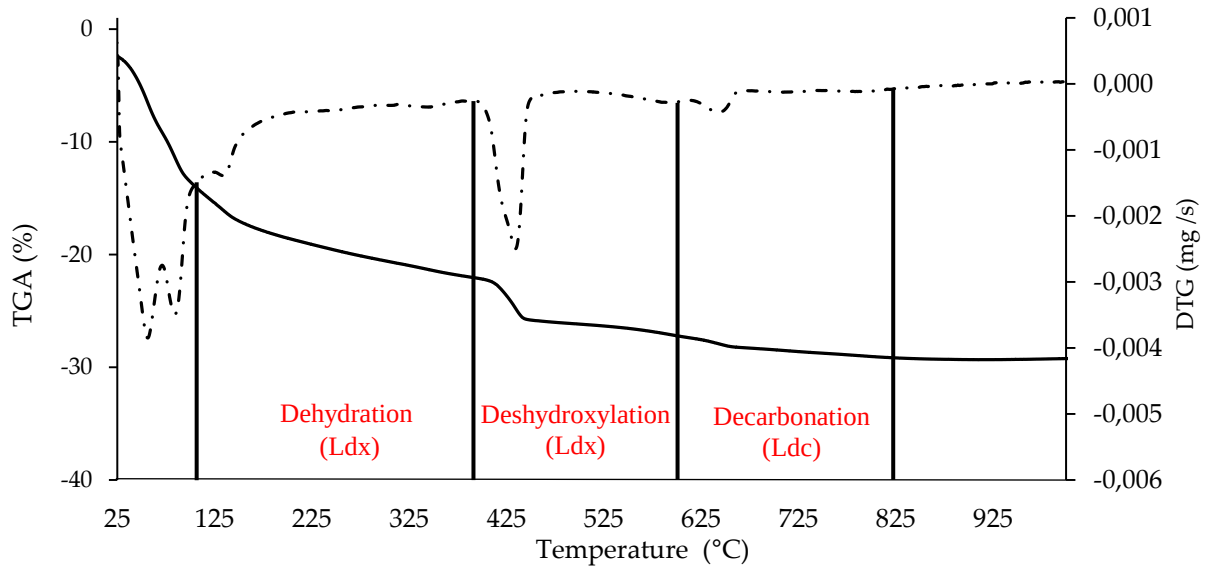

Fig. 3: TGA and DTG of P10RP mixture

The methodology used in the present paper has been suggested by Deboucha et al. [24], [29]. The calculation of the degree of hydration of cement paste with or without additives (RP or LF) is given as follows:

$$\alpha = \frac{W_B(t)}{W_{B\infty} \times L_{eq}} \quad (1)$$

where $W_B(t)$ is the mass of chemically bound water at time t; $W_{B\infty}$ is the ultimate chemically bound water per mass of binder; L_{eq} is the equivalent mass of binder. The bound water at time t was calculated as follows:

$$W_B(t) = Ldh + Ldx + 0.41\,(Ldc - Ldc_a) - (m_c\,LOI_{cc} + m_a\,LOI_{ac}) + m_d \quad (2)$$

where Ldh, Ldx, Ldc and Ldc_a are the mass loss between 105 and 400 °C, 400 and 600 °C, 600 and 800 °C and the mass loss for anhydrous materials (recycled powder, limestone filler and cement) between 600 and 800 °C respectively.

m_c and m_a are respectively the mass of cement and additions in the sample, which were calculated according to the equations given by Deboucha et al. [24].

m_d is the device's drift equal to m_d= 0.29 mg, similarly to that obtained by Deboucha and Mounanga for the same device [28], [30]. LOI_{cc} and LOI_{ac} are the mass loss of anhydrous materials between 105 and 600 °C for cement and additives respectively (see Table 4).

$W_{B\infty}$ is the ultimate chemically bound water per gram of binder. It represents the quantity of water necessary for a complete hydration of different clinker phases. A value of $W_{B\infty}$ equal to 0.23 *i.e.* 0.23 g of water is required to completely hydrate 1 g of pure Portland cement [30].

L_{eq} is the equivalent mass of binder that takes into consideration the contribution of additions to the hydration reactions [24]. It is given by following relationship:

$$L_{eq} = m_c + k\, m_a \quad (3)$$

where k is the activity coefficient calculated according to equation (4) [29]. It allows to estimate the contribution of the quantity of mineral addition on the hydration reaction by accounting for the activity index I. The later was determined according to the standard NF P 18-508 [31].

$$k = 3I - 2 \quad (4)$$

The values of k for recycled powder and limestone filler are presented in Table 5.

Table 4 : Mass loss for anhydrous materials

Anhydrous Materials	$m_{105°C\text{-}600°C}$ (%)	$m_{600°C\text{-}950°C}$ (%)
Portland cement	0.86	0.28
Recycled powder	2.65	7.2
Limestone filler	0.65	42.3

Table 5 : Activity coefficient k for used mineral additions

Mineral Addition	Coefficient k
Recycled powder (RP)	0.43
Limestone filler (LF)	0.26

2.3.3. Mechanical properties

The compressive and flexural strength tests were performed on 40x40x160 mm^3 prisms according to the standard NF EN 196-1 [26] at 3, 7, 28 and 90 days. The dynamic Young modulus was determined using a Grindosonic® apparatus on cement paste and mortar samples. The measurement is a non-destructive method based on the flexural resonant frequency to an impulsion and performed according to the standards ASTM E1876-15 and NF EN ISO 12680-1 [32],[33]. Elastic dynamic modulus is calculated with equation (5) based on the measured flexural resonant frequency, the dimensions and the mass of the test specimen:

$$E = 0.9465 \left[\frac{m\, f_f^2}{b}\right]\left[\frac{L^3}{t^3}\right] T_1 \quad (5)$$

Where E is the Young modulus (Pa); m is the mass of the specimen (g); b, L and t are its width, length and thickness (mm) respectively; f_f is the fundamental resonant frequency (Hz) and T_1 is the correction factor for fundamental flexure.

2.3.4. Water porosity

The porosity accessible to water of mortars was determined at 7, 28 and 90 days according to the standards NF P 18-459 and the GranDuBé recommendation [34],[35]. Measurements were carried out on three 40x40x80mm^3 prismatic specimens for each mortar mix to ensure a good repeatability, by splitting 40x40x160mm^3 prism in a 3-point bending test. These prisms have undergone no specific surface treatment is done after demolding. First, the samples were put in a desiccator and subjected to a vacuum pressure of 0.25 bar for 4 hours. By keeping the vacuum pressure, they were immersed at first up to half height with water for 44 hours, and then totally immersed for 24 hours. At the end, each sample was weighed in water and in air respectively. For weighing in air, the surface of the samples is wept with a wet handkerchief. They were finally oven-dried at 105 °C until stabilization of the mass is reached. The porosity accessible to water P_w is calculated as follows:

$$P_w = \frac{M_{air} - M_{dry}}{M_{air} - M_{hyd}} \quad (6)$$

with M_{air} the mass of the saturated sample (g); M_{dry} the mass of the dried sample (g); M_{hyd} the hydrostatic mass of the sample (g).

2.3.5. Mercury intrusion porosimetry

The mercury intrusion porosimetry (MIP) technique allows to characterize the pore size distribution. Tests were carried out on 4-6 cm^3 prismatic specimens extracted from 40x40x160 mm^3 prisms. The latter were dried at 40°C for 2 weeks until mass stabilization, then were taken out of oven and placed at 20°C in a desiccator filled with silica gel until a constant mass is reached.

An AutoPore IV 9500 apparatus was used. It allows to apply maximal mercury injection pressure of 228 MPa. The investigated pores diameter ranges 360 µm to 6 nm. The Washburn equation relates the pressure to the pore diameter by [36]:

$$d_p = \frac{-4\,\gamma\,cos\,\theta}{p} \quad (7)$$

where γ is the surface tension of mercury equal to 0.485 N.m^{-1}, θ is the contact angle equal to 130°, p is the mercury injection pressure.

2.3.6. Gas permeability

The gas permeability was measured by using CEMBUREAU method at 28 and 90 days respectively. Tests were performed on cylindrical samples of 70 mm diameter and 50 mm thickness to ensure a good repeatability of measurements. The latter were dried at 80 °C until stabilization of the mass as a recommended by GranDuBé [12] and kept at 20°C in a desiccator filled with silica gel one day before measurements.

Four different inlet pressures were applied from 4 to 1 bar above atmospheric pressure to account for Klinkenberg's effect. The outlet pressure is equal to the atmospheric one. In the case of laminar flow, the apparent gas permeability K_a can be calculated from Darcy equation and the mass balance equation combined with the law of ideal gases as follows:

$$K_a = \frac{2\,P_o Q L \mu}{A({P^2}_{in} - {P^2}_o)} \tag{8}$$

With P_{in} (Pa) is the inlet pressure; P_o is the outlet pressure (atmospheric pressure); Q is the gas flow ($m^3.s^{-1}$); L is the thickness of the sample (m); A is the section (m^2); μ is the nitrogen dynamic viscosity at 20°C ($1.75x10^{-5}$ Pa.s).

The intrinsic permeability K_{int}(m^2) is deduced from the apparent one by considering the Klinkenberg's effect as follows:

$$K_a = K_{int}\left(1 + \frac{\beta}{P_m}\right) \tag{9}$$

where P_m(Pa) is the average gas pressure between P_o and P_{in} and β is the Klinkenberg coefficient which allows to distinguish the contribution of slip flow on small pore walls from that of viscous flow.

3. Multi-scale modeling

A multi-scale model is developed to gain insight on the effect of partial cement replacement by RP or LF on the mechanical properties of cement pastes and mortars

3.1. Homogenization schemes for elastic moduli

3.1.1. Principles of homogenization in continuum micromechanics

Let us briefly recall the principles of homogenization in continuum micromechanics, additional details can be found in e.g. [37],[38],[39]. At a microscopic scale, cement paste or mortar appear as heterogeneous materials with heterogeneous stiffness fields $\mathbb{C}$. A Representative Volume Element (RVE) of a heterogeneous material is defined as a volume small compared to the macroscopic scale and large compared to the size of the heterogeneities. In what follows, RVEs of different materials are considered at multiple levels or length scales: one for the mortar, one for the cement paste, and one for a so-called hydrate foam within the cement paste (see Fig. 4).

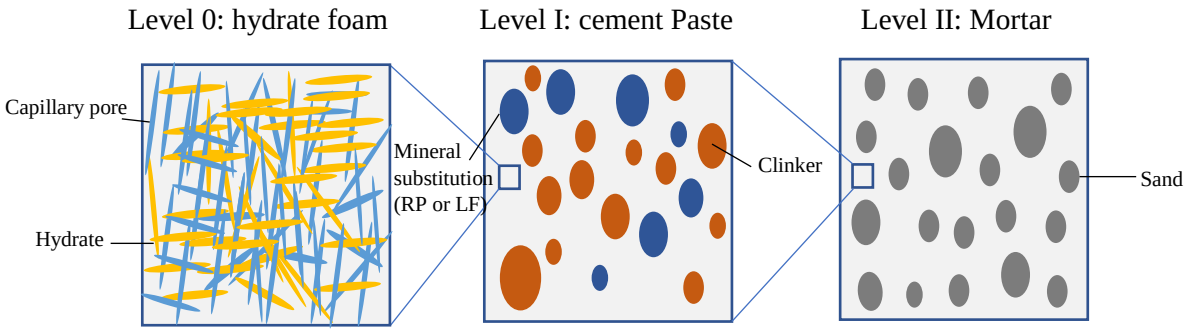

Fig. 4 : schematic representation of the model of cement paste and mortar across three length scales

At each level, an RVE comprises n phases (i.e. constituents). For instance, at level II the mortar comprises cement paste and sand. Each phase $i \in [1, \ldots, n]$ has a volume fraction f_i and a uniform stiffness $\mathbb{C}_i$, with $\sum_{i=1}^{n} f_i = 1$. Let us denote by $\langle F \rangle_i$ the intrinsic volume average over a phase i of any field F and $\langle F \rangle = \sum_{i=1}^{n} f_i \langle F \rangle_i$ its volume average over the RVE.

The application of a macroscopic strain $\overline{\epsilon}$ on the RVE develops heterogeneous microscopic strain ϵ and stress $\sigma = \mathbb{C}:\epsilon$ fields within the RVE. These non-uniform fields are related to the macroscopic strain $\overline{\epsilon}$ by a field of strain concentration $\mathbb{A}$ (fourth order tensor), defined such as $\epsilon = \mathbb{A}:\overline{\epsilon}$ and hence $\sigma = \mathbb{C}:\mathbb{A}:\overline{\epsilon}$. Typically, soft (resp. stiff) regions will have strain concentrations above (resp. below) unity. The strain and stress averaging rules ensure that $\overline{\epsilon}$ and $\overline{\sigma}$ correspond to the macroscopic strain and stress respectively, which entails $\langle \mathbb{A} \rangle = \sum_{i=1}^{n} f_i \langle \mathbb{A} \rangle_i = \mathbb{I}$ where $\mathbb{I}$ denotes the fourth order identity tensor.

The effective stiffness of the RVE, which relates the macroscopic quantities via $\overline{\sigma} = \mathbb{C}^{hom}:\overline{\epsilon}$ by definition is then $\mathbb{C}^{hom} = \langle \mathbb{C}:\mathbb{A} \rangle = \sum_{i=1}^{n} f_i \mathbb{C}_i \langle \mathbb{A} \rangle_i$. To determine this homogenized stiffness, one must hence determine the phase-wise averages $\langle \mathbb{A} \rangle_i$ of the strain concentration tensors in addition to knowing the stiffness and volume fraction of each phase. Classical methods to estimate these $\langle \mathbb{A} \rangle_i$ based on the solution to the Eshelby problem are briefly recalled below.

3.1.2. Eshelby problem

The Eshelby inhomogeneity problem [40] is defined on an infinite reference medium of uniform stiffness $\mathbb{C}_0$ in which a single inclusion i with stiffness $\mathbb{C}_i$ is embedded. A remote strain $\boldsymbol{\epsilon}_\infty$ is enforced infinitely far from the inclusion. If the inclusion is of ellipsoidal shape, the strain in the inclusion ϵ_i is constant and calculated using the Hill tensor $\mathbb{P}_0^i$ as follows:

$$\epsilon_i = \mathbb{A}_0^i : \boldsymbol{\epsilon}_\infty = \left[\mathbb{I} + \mathbb{P}_0^i : (\mathbb{C}_i - \mathbb{C}_0)\right]^{-1} : \boldsymbol{\epsilon}_\infty \quad (10)$$

The Hill tensor $\mathbb{P}_0^i$ is a fourth order tensor which depends on the stiffness $\mathbb{C}_0$ and on the shape and orientation of the inclusion i. It is related to the fourth order Eshelby tensor $\mathbb{S}_0^i$ by $\mathbb{P}_0^i = \mathbb{S}_0^i:\mathbb{C}_0^{-1}$. $\mathbb{A}_0^i$ is the concentration tensor of the Eshelby inhomogeneity problem [38], [41], and is used in homogenization schemes as a building brick to derive estimates of $\langle \mathbb{A} \rangle_i$, as sketched below.

3.1.3. Matrix-inclusion composites

The Mori-Tanaka scheme is appropriate for materials which have a matrix m phase in which there are several inclusions of different phases i. Each type of inclusion is represented by corresponding Eshelby

inhomogeneity problem with a choice of ellipsoidal shape representative of the actual inclusion shape. The Mori-Tanaka estimate of the homogenized stiffness as follows [42], [43] :

$$\mathbb{C}_{mt} = \langle \mathbb{C}_i : \mathbb{A}_m^i \rangle : \langle \mathbb{A}_m^i \rangle^{-1} \tag{11}$$

with $\langle \mathbb{A}_m^i \rangle$ the Eshelby concentration tensor of each inclusion phase $i \neq m$ in the reference medium of stiffness $\mathbb{C}_0 = \mathbb{C}_\mathrm{m}$, and by extension $\mathbb{A}_m^m = \mathbb{I}$ for the matrix phase m.

3.1.4. Poly-Crystalline or disordered composites

The self-consistent scheme [44] is used for disordered composites where there is no matrix phase. The self-consistent scheme takes into consideration the shape and volume fraction of each phase, as the Mori Tanaka scheme. The self-consistent scheme allows taking into account approximately the percolation process of the solid and pore phases [41]. The self-consistent scheme assumes that particles of each phase i can be represented by an Eshelby inhomogeneity embedded in the homogenized composite, i.e. the reference stiffness is implicitly defined as $\mathbb{C}_0 = \mathbb{C}_{sc}$ where $\mathbb{C}_{sc}$ is the self-consistent estimate of the homogenized stiffness $\mathbb{C}_{hom}$. $\mathbb{C}_{sc}$ is then the solution to the following tensor equation:

$$\mathbb{C}_{sc} = \langle \mathbb{C}_i : \mathbb{A}_{sc}^i \rangle : \langle \mathbb{A}_{sc}^i \rangle^{-1} \Leftrightarrow \langle (\mathbb{C}_i - \mathbb{C}_{sc}) : \mathbb{A}_{sc}^i \rangle = 0 \tag{12}$$

with $\mathbb{A}_{sc}^i$ the Eshelby concentration tensor of each phase in the reference medium of stiffness $\mathbb{C}_0 = \mathbb{C}_{sc}$.

3.2. Morphological model of cement pastes and mortar

The multi-scale morphological model chosen to study the mechanical properties is inspired from the so-called engineering micromechanics model first proposed by Pichler and Hellmich [45], and latter adapted by Achour et al. [41]. These models can be used in combination with the hydration model of Powers and Brownyard [46]. The present model features three scales for mortars, including two for cement paste (see Fig. 4). The smallest scale corresponds to a hydrate foam (Level 0), the second to a cement paste (Level I), and the last to a mortar (Level II), defined as follows:

- Level 0: The hydrate foam is defined as a disordered mix of hydrates and capillary pores. It is modeled using the self-consistent scheme with isotropically oriented spheroidal inhomogeneities representing the hydrates and the capillary pores.

- Level I: The cement paste is represented as a matrix-inclusion composite with inclusions of clinker or mineral additions (LF or RP) embedded in a matrix of hydrate foam. It is modeled using the Mori-Tanaka scheme with anhydrous clinker and mineral additions represented by spherical inhomogeneities.

- Level II: The mortar is represented as a matrix-inclusion composite with inclusions of sand embedded in a matrix of cement paste. It is modeled using the Mori-Tanaka scheme with sand grains represented by spherical inhomogeneities.

3.3. Hydration model

The model used to estimate the volume fraction of each constituent in the cement paste as a function of the degree of hydration is an adaptation of the hydration model of Powers and Brownyard [46] with the

consideration of substitution rates of additions. The degree of hydration of the clinker $\alpha_{clinker}$ is defined as the mass percentage of anhydrous clinker that has been hydrated with water. Powers' model is a simplified model that gives us the volume fractions of hydrates (f_h), anhydrous clinker (f_a) and capillary pores (f_{cp}) at the level of cement paste, as a function of the water to binder ratio and of the degree of hydration $\alpha_{clinker}$ [46]. The parameters needed to determine these volume fractions are the volume of hydrate $k_h = 2.13$ formed and the volume of water $k_w = 1.31$ consumed for a complete hydration of a quantity of clinker, the density of anhydrous clinker $\rho_a = 3.12$.

In the case of mineral substitutions, the volume fraction of substitution (f_s) in the cement paste is a function of the substitution rate X expressed in mass percentage, the density of additions and the effective water to binder ratio. Additional required parameters are the density of substituted additions ρ_s, equal to 2.7 for limestone filler and 2.3 for recycled powder. Assuming that the substituted mineral additions do not react with clinker, the volume fractions of each constituents of cement paste are calculated as follows:

$$f_s = \frac{X\,\rho_a}{X\,\rho_a + (1-X)\,\rho_s\,\left(1+\rho_a\ w/c_{eff}\right)} \tag{13}$$

$$f_a = (1-\ f_s)\ \frac{1-\alpha_{clinker}}{1+\rho_a\, w/c_{eff}} \tag{14}$$

$$f_h = (1-\ f_s)\ \frac{k_h\,\alpha_{clinker}}{1+\rho_a\ w/c_{eff}} \tag{15}$$

$$f_{cp} = (1-\ f_s)\ \frac{\rho_a\ w/c_{eff} + (1-k_h)\alpha_{clinker}}{1+\rho_a\ w/c_{eff}} \tag{16}$$

$$w/c_{eff} = \frac{w/b_{eff}}{1-X} \tag{17}$$

Where w/c_{eff} is the effective water-to-cement ratio and w/b_{eff} is the effective water-to-binder ratio available for hydration. The later can be lower than w/b for two reasons: part of the mix water can be absorbed by mineral substitutions if they are porous, and another part can react with the mineral substitution if they are reactive with water. Both situations are encountered for RP, as will be later (see equation 18).

According to Powers and Brownyard [46], the total porosity in the cement paste is equal to $0.28\ f_h + f_{cp}$. Hence, in the case of substituted mineral additives with porosity $\phi_s$the cement paste porosity should be $0.28\ f_h + f_{cp} + \phi_s f_s$. Powers' model does not provide the evolution of the degree of hydration with time. The maximum degree of hydration, reached when either clinker or water is depleted or no more capillary space is available, depends on the water-to-cement ratio and on the availability of external water during curing [41].

3.4. Model parameters

The model parameters are summarized in Table 6. A chart of the homogenization workflow is provided in Fig. 5

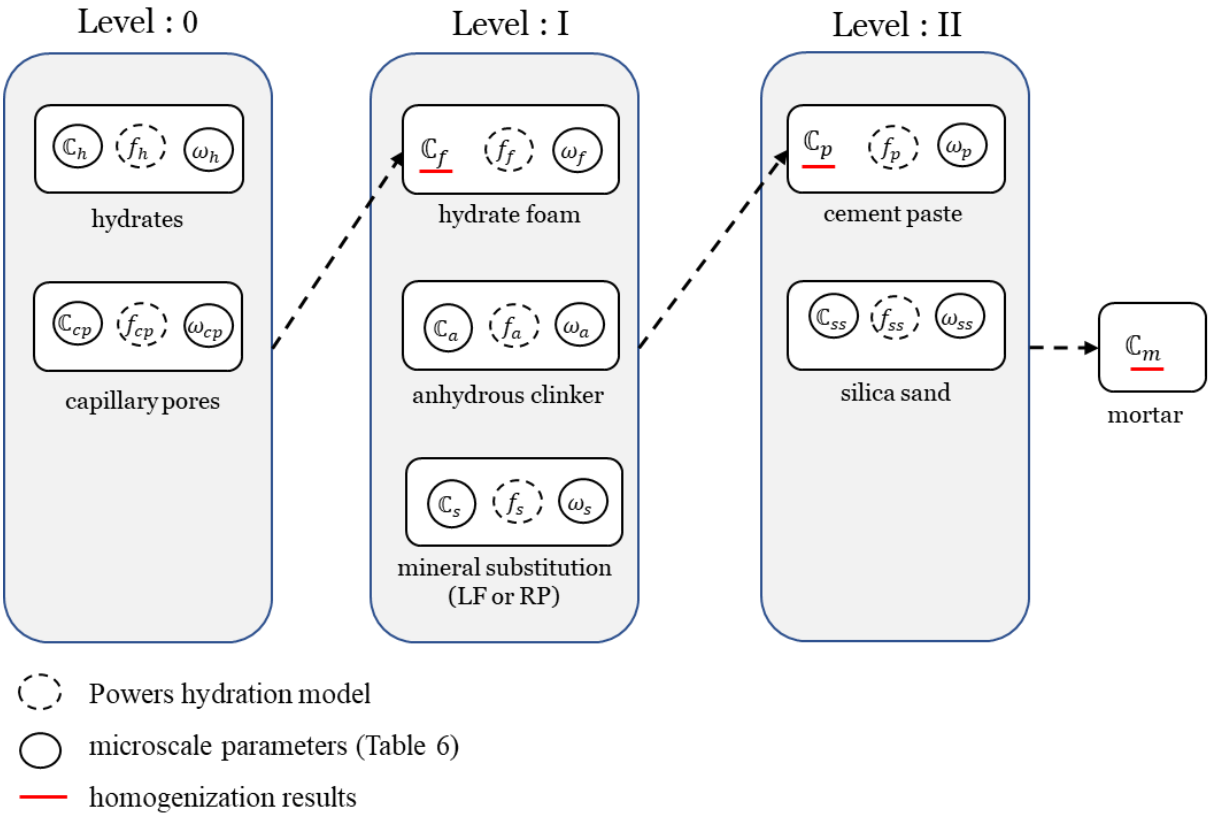

Fig. 5 :Flowchart of calculations for the model

Level 0: Model parameters for the hydrate foam are of geometrical and mechanical nature:

- Geometrical parameters: The aspect ratio ω_h and ω_{cp} of the spheroidal inhomogeneities used to represent the hydrate particles and the capillary pores respectively. These model parameters are set to $\omega_h = 0.013$ and $\omega_{cp} = 6$ as in Achour et al. [41].
- Mechanical parameters: The stiffness tensors of each phase. The capillary pore stiffness is zero, while the stiffness tensor of the hydrates is assumed isotropic, with Young's modulus $E_h = 35\,GPa$ and Poisson ration $\upsilon = 0.30$ to bulk and shear moduli $k_h = 29.2\,GPa$ and $\mu_h = 13.5\,GPa$ respectively from Bernard et al., and P. Acker [47], [48]. Note that several different values of the hydrate stiffness have been reported in literature [41], [45], [47]–[49]. The value chosen here has been selected as it provides a good agreement with measured stiffness on the reference cement paste PR.

Level 1: Since anhydrous clinker and mineral additions are represented by spherical inhomogeneities, the model parameters are of mechanical nature (see Table 6):

- Hydrate foam: The stiffness tensor is isotropic with bulk and shear moduli k_f and μ_f obtained by homogenization using the self-consistent scheme from level 0.

- Anhydrous clinker: The stiffness is assumed isotropic with bulk and shear moduli $k_a = 112.5\ GPa$ and $\mu_a = 51.9\ GPa$ from [48].
- Limestone Filler: LF are assumed inert and non-porous particles, with bulk and shear moduli $k_{LF} = 73.3\ GPa$ and $\mu_{LF} = 32.0\ GPa$ from [50] for calcite.

- Recycled Powder: RP particles are so fine that their stiffness and porosity can hardly be obtained experimentally. Further RP particles are not inert as there remains an anhydrous fraction within the old cement paste. To overcome these difficulties, the following approximation and assumptions are adopted: RP particles are modeled as mostly old cement paste particles. whose properties will be estimated from the present model. This is obviously a strong assumption, which could be improved in future works to account for the presence of residual fine crushed aggregate in RP that is likely from the chemical compositions listed in Table 1. It is assumed that this old cement paste has been cast with a water-to-cement ratio 0.4, as an approximation of actual values used for on-site mixes. Before use in a new cementitious material, the old paste coming from the construction and demolition wastes has not reached its ultimate hydration degree. Indeed, a measurement of the total heat of hydration released by mixture of the recycled powder with water revealed a total heat release equal to 47 J/g of RP, which remains stable after 24 hours. This release is approximately 10% of the total hydration heat of a freshly cast cement paste. It is further assumed that the old paste had previously reached a degree of hydration around 85%, and will hydrate by an increment $\Delta\alpha = 10\%$ up to 95% in the 24h following its reuse in a fresh paste. As a result, the modeled porosity of RP before new hydration is estimated to $\phi_{RP} = 36\%$ according to Powers hydration model. After rehydration up to a degree of hydration of 95%, the RP stiffness modeled from the present multi-scale model without substitution has a bulk modulus $k_{RP} = 23.0\ GPa$ and shear modulus $\mu_{RP} = 11.5\ GPa$. The effective water-to-binder ratio available for new clinker hydration is then estimated as a function of the substitution rate X by RP by mass as:

$$w/b_{eff} = w/b - X \times \left(\frac{\phi_{RP}}{\rho_{RP}} + \frac{k_w \Delta\alpha}{\rho_a}\right) \tag{18}$$

where the first term in the parenthesis concerns the water absorbed in the RP porosity and the second one the water consumed by the increment in hydration reaction of the old clinker from RP.

Level II: Silica sand grains are represented by spherical inclusions with the bulk and shear moduli equal to k_{ss} = 37.9 GPa and μ_{ss} = 44.3 GPa from [45] for quartz.

Table 6: Microstructural parameters of the multiscale model: elastic moduli and aspect ratio of the different phases

Phase	Bulk modulus	Shear modulus	Reference	Aspect ratio
	k [GPa]	μ [GPa]		ω [-]
Anhydrous clinker	112.5	51.9	[49]	1

Limestone filler	73.3	32	[50]	1
Recycled powder	23.0	11.5	from model	1
Capillary pores	0	0	[47]	6
Hydrates	29.2	13.5	[47]	0.013
Sand	37.9	44.3	[45]	1

3.5. Computation of the homogenized stiffness

The stiffness tensor has been estimated following a step-by-step approach at each level up to the mortar, see Fig. 5.

At level 0. The stiffness for the hydrate foam was estimated by the self-consistent scheme by solving the equation (12), following the mathematical details provided in [41], Appendix A. The upscaled foam properties vary as a function of the intrinsic capillary porosity of the foam given by the ratio $f_{cp}/(f_{cp}+f_h)$. This ratio is obtained from Powers' model and depends on the effective water-to-cement ratio and degree of hydration.

At level I. The stiffness tensor is estimated using the Mori-Tanaka scheme. The projection of equation (11) on the spherical and deviatoric isotropic fourth order tensors gives the following expression of the Mori-Tanaka estimate of the bulk and shear moduli k_p and μ_p of cement paste:

$$k_p = k_f\left[1+\frac{x}{1-\alpha_f x}\right] \tag{19}$$

$$where\ x=\sum_{i=a,s}\frac{f_i(k_i-k_f)}{k_f+\alpha_f(k_i-k_f)}\quad with\ \alpha_f=\frac{3k_f}{3k_f+4\mu_f}$$

$$\mu_p = \mu_f\left[1+\frac{y}{1-\beta_f y}\right] \tag{20}$$

$$where\ \ y=\sum_{i=a,s}\frac{f_i(\mu_i-\mu_f)}{\mu_f+\beta_f(\mu_i-\mu_f)}\quad with\ \beta_f=\frac{6}{5}\frac{k_f+2\mu_f}{3k_f+4\mu_f}$$

where α_f and β_f are the components of the Eshelby tensor of a sphere in an isotropic reference medium with bulk and shear moduli k_f and μ_f [41].

At level II. The stiffness tensor is estimated using the Mori-Tanaka scheme. The projection of equation (11) on the spherical and deviatoric isotropic fourth order tensors yields us the following expression of the Mori-Tanaka estimate of the bulk and shear moduli k_m and μ_m of mortar:

$$k_m = k_p\left[1+\frac{x_{ss}}{1-\alpha_p x_{ss}}\right] \tag{21}$$

$$where\ x_{ss}=\frac{f_{ss}(k_{ss}-k_p)}{k_p+\alpha_p(k_{ss}-k_p)}\quad with\ \ \alpha_p=\frac{3k_p}{3k_p+4\mu_p}$$

$$\mu_m = \mu_p \left[1 + \frac{y_{ss}}{1 - \beta_p y_{ss}}\right] \quad (22)$$

$$where\ y_{ss} = \frac{f_{ss}(\mu_{ss} - \mu_p)}{\mu_p + \beta_p(\mu_{ss} - \mu_p)}\ \ with\ \ \beta_p = \frac{6}{5}\frac{k_p + 2\mu_p}{3k_p + 4\mu_p}$$

Model results are presented in section 4.3 along with experimental results for a direct comparison.

4. Results and discussion

4.1. Hydration

4.1.1. Heat of hydration

Table 7 presents the total heat of hydration (per gram of binder) of blended cement pastes (PR, P10RP, P10LF, P20RP and P20LF) during the first 120h of hydration under isothermal conditions (T=20°C). The corresponding heat rates are shown in Fig. 6. It is observed that the shape of the heat of hydration profile of blended mixtures is similar to that of the reference paste whatever the replacement rate and the nature of addition. Concerning the PR mixture which is considered as the reference, the principal peak of heat rate is measured at 10h with an intensity value equal to 3.6 mW/g. The relative values of the principal peak obtained for P10RP, P10LF, P20RP and P20LF are 90%, 89%, 80% and 83% respectively in comparison with PR mixture. The relative values of the principal peak of heat hydration indicate that use of RP or LF as cement replacement caused a decrease in the heat rate during the first hours of hydration due to dilution effect [24],[51].

As shown in Table 7 and Fig. 6, the principal peaks of heat hydration for cement pastes containing RP or LF shifted slightly to the left of PR indicating that the presence of RP or LF fine particles can accelerate the hydration process of cement through the heterogeneous nucleation effect. In fact, several studies reported that mineral additive's fine particles can act as a nucleation site for the hydration products of cement [24],[28],[29].

Fig. 6 also provides the total heat released for the reference cement paste and pastes prepared with RP or LF. It is clear from this figure that the total heat released decreased when the replacement levels of cement by RP or LF increased. The total heat of pastes prepared with RP or limestone filler was found in the range of 93-87% of the pure cement paste. These results are in good agreement with literature review where it is known that the addition of mineral additives such as limestone filler in binder decreases to total heat releases due to dilution effect [28],[52].

Table 7 shows also the total heat released for pastes studied after 10, 24 and 120 hours of hydration. It can be clearly seen that with increasing curing time, the difference in the response of total heat released between the reference cement paste and pastes prepared with RP or LF was decreased. Indeed, after 10 hours of hydration, the total heat released of cement pastes prepared with RP or LF was in the range of 92-85 % of the PR. Meanwhile, after 120 hours of hydration, the total heat released of cement pastes prepared with RP or LF was in the range of 93-87 % of the PR. The enhancement in the total heat with increasing curing for time cement pastes prepared with LF could be explained through the hemi- and monocarboaluminate formation where the calcium carbonate present in LF can react with aluminate phase present in cement to form hemi- and monocarboaluminate [29]. For RP cement pastes, the enhancement in the total heat released with curing time might be might be due to the reactivity of residual clinker present in RP grains.

Table 7 : Characteristic values of isothermal calorimeter tests

Mix	Age of hydration peak	Intensity of hydration peak	Total heat (10 h)	Total heat (24 h)	Total heat (120 h)

	Measured values (h)	Relative values (%)	Measured values (mW/g)	Relative values (%)	Measured values (J/g)	Relative values (%)	Measured values (J/g)	Relative values (%)	Measured values (J/g)	Relative values (%)
PR	10.01	100	3.60	100	102.95	100	232.79	100	364.18	100
P10RP	9.54	98.9	3.25	90.27	91.69	89.06	215.84	92.71	340.12	93.39
P10LF	9.48	97.9	3.20	88.89	94.6	91.89	219.58	94.32	339.60	93.25
P20RP	9.49	98	2.88	80	90.45	87.86	205.42	88.24	321.69	88.33
P20LF	9.25	94	2.97	82.5	88.07	85.55	206.84	88.85	318.39	87.43

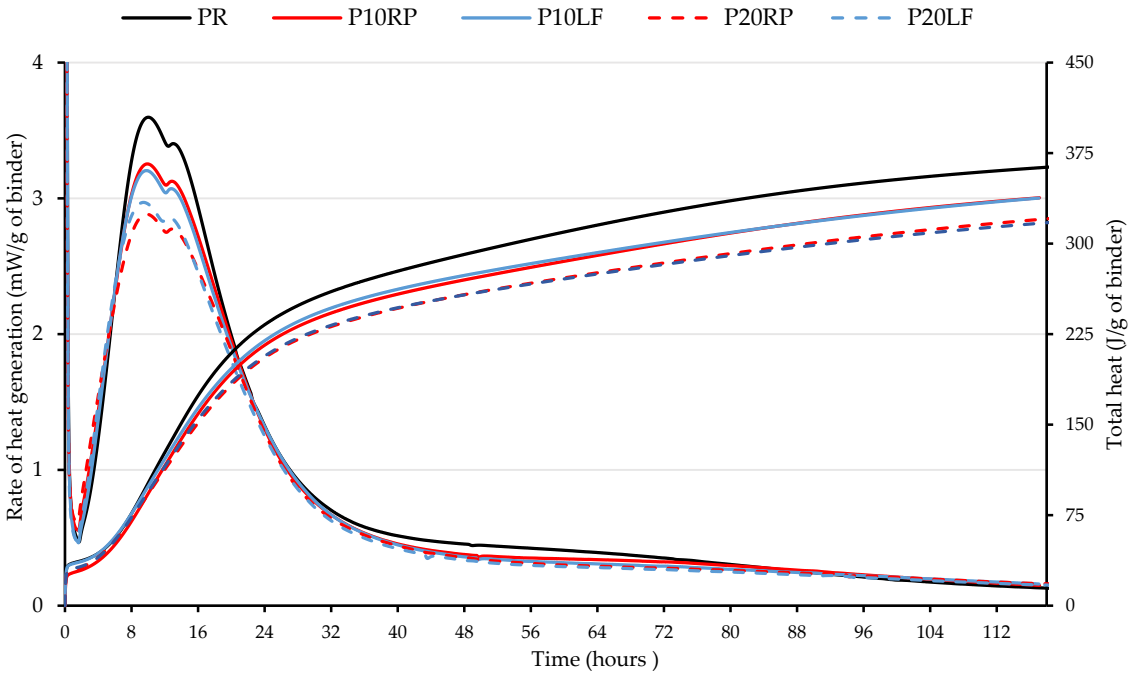

Fig. 6 : Hydration heat of the reference paste and the cement paste containing RP or LF

4.1.2. Degree of hydration

For all cement paste mixtures, the evolution of mass versus temperature at 3, 7, 28 and 90 days respectively, are shown in Table 8. The temperature values reported in Table 9 correspond to those involved in the calculation of degree of hydration as given by equation (1). Estimated hydration degrees and its relative values to the reference paste at the same ages are provided in Table 9.

Fig. 7 shows the evolution of the hydration degree over time for ~~the~~ blended cement pastes containing recycled powder or limestone filler It is clear that, at all testing ages, the degree of hydration of PR is higher than the other mixtures prepared with RP or LF. It is also observed that the hydration degree decreased with increasing replacement levels of cement by RP or LF. For instance, at 3 and 7 days, the decrease in the hydration degree for cement paste prepared with 10% RP was found to be 18 and 12 % respectively. Similarly, the decrease in the hydration degree for cement paste prepared with 20 % RP was found to be 25 and 20 % respectively. The decrease in the hydration degree is directly due to dilution effect as pointed out by [51], [53].

Referring to previous studies on the effect of limestone filler on the hydration of cement paste [24], [28], [29],[54], the addition of limestone filler with low replacement levels (5%) can enhance the long-term hydration degree of cement paste. Indeed, Deboucha et al. [24] found that, after 90 days of hydration, the degree of hydration of cement paste prepared with 5 % LF was slightly higher by about 2% when compared to the reference cement paste's hydration degree, due to the formation of hemi- and monocarboaluminate phases. However, in this study, the lower replacement level selected is 10% which means that the formation of hemi- and monocarboaluminate phases at later ages cannot compensate for lower hydrate products of cement due to dilution effect.

Regarding the effect recycled powder on the hydration degree development, as mentioned above (Sec. 4.1.1), the addition of RP to Portland cement can enhance the hydration kinetic through the reactivity of residual clinker present in RP and the heterogeneous nucleation. However, further research is needed, taking into consideration other parameters such as replacement levels and particles size distribution to give a general overview on the impact of RP on hydration

Table 8: Mass loss values during TGA tests

Mix	Age(days)	M_{sample}	$M_{105°C}$	$M_{400°C}$	$M_{600°C}$	$M_{800°C}$
PR	3	22.9984	19.1897	18.0737	17.1260	16.8740
	7	22.9977	19.5582	18.1927	17.3041	17.0777
	28	22.9985	20.2090	18.9252	17.8299	17.3635
	90	22.9985	19.6201	17.7617	16.6612	16.5361
P10RP	3	22.9979	18.5890	17.5894	16.6743	16.4190
	7	22.9984	18.3703	17.2999	16.1495	15.7676
	28	22.9990	19.2205	18.1605	16.8767	16.6354
	90	22.9985	19.3688	17.9791	16.7418	16.2763
P10LF	3	20.9980	17.0609	16.3425	15.4753	14.6091
	7	22.9982	18.8622	17.9991	16.9597	16.0844
	28	22.9978	20.0524	19.0177	17.6800	16.8403
	90	22.9995	19.2174	17.7558	16.6630	15.7262
P20RP	3	23.9973	19.3686	18.2896	17.6162	17.2474
	7	21.9974	17.3683	16.3801	15.5118	15.1467
	28	22.9980	19.2434	18.2452	17.2798	16.6302
	90	22.9984	19.1505	17.6279	16.9197	16.2338
P20LF	3	20.9973	17.2417	16.6442	15.9258	14.6757
	7	20.9976	16.9946	16.1768	15.3667	14.0569
	28	22.9977	19.2875	18.0761	17.2392	15.5962
	90	22.9976	18.7817	17.7412	16.6578	15.1218

Table 9 : Measured mass losses Ldh, Ldx, Ldc, Ldca, W_B and computed overall hydration degree α

Mix	Age (days)	Ldh (mg)	Ldx (mg)	Ldc (mg)	Ldca (mg)	W_B (mg)	α (%)	α / α_{PR} (%)
PR	3	1.1160	0.9477	0.2520	0.0424	2.2792	65.37	100
	7	1.3655	0.8886	0.2264	0.0424	2.4592	70.53	100
	28	1.2838	1.0953	0.4664	0.0424	2.6825	76.94	100
	90	1.8584	1.1005	0.1251	0.0424	3.1224	89.55	100
P10RP	3	1.0774	0.8373	0.2553	0.1326	1.7332	53.41	82
	7	1.1331	1.0877	0.3819	0.1326	2.0073	61.85	88

	28	1.0771	1.2667	0.2413	0.1326	2.1144	65.15	85
	90	1.5278	1.0992	0.4655	0.1326	2.3482	72.36	81
P10LF	3	0.7184	0.8672	0.8662	0.6115	1.7204	53.73	82
	7	0.8631	1.0394	0.8753	0.6115	1.9181	59.90	85
	28	1.0347	1.3377	0.8397	0.6115	2.0636	64.44	84
	90	1.4616	1.0928	0.9368	0.6115	2.3378	73.01	82
P20RP	3	1.0790	0.6734	0.3688	0.2106	1.5343	48.95	75
	7	0.9882	0.8683	0.3651	0.1930	1.6126	56.13	80
	28	0.9982	0.9654	0.6496	0.2018	1.9729	65.68	85
	90	1.5226	0.7082	0.6859	0.2018	2.0863	69.46	78
P20LF	3	0.5975	0.7184	1.2501	0.9615	1.3029	48.91	75
	7	0.8178	0.8101	1.3098	0.9615	1.5723	59.03	84
	28	1.2114	0.8369	1.6430	1.0531	1.8818	64.50	84
	90	1.0405	1.0834	1.5360	1.0531	1.9796	67.85	76

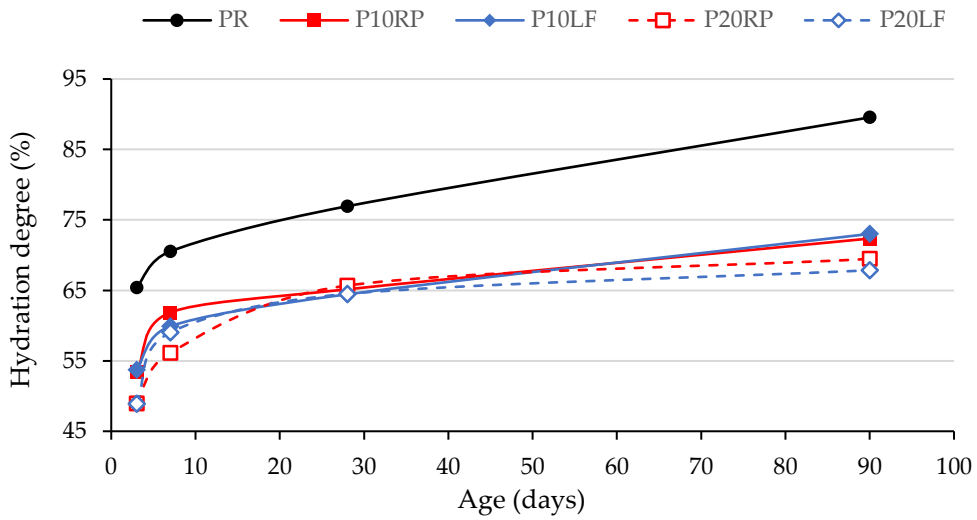

Fig. 7 : Hydration degree of the reference paste and cement paste containing RP or LF

4.2. Pore structure and transport properties

4.2.1. Water porosity

The water porosity test was carried out on three specimens of 40x40x80 mm^3 at 7, 28 and 90 days. Fig. 8 shows the evolution of the total porosity for the reference mortar and mortars prepared with RP and LF. A decrease in the total porosity with time for all mortars is observed. This is due to the increase in the hydration degree and to the progressive filling of large pores with hydration products [55]. From Fig. 8, it is clear that the replacement of cement by RP or LF increases the total porosity at all testing ages (early and later age). This corroborates the dilution effect and the drop in the density of the binder as observed in Table 3.

At 7 days, mortars incorporating RP exhibited a slightly higher total porosity values compared to the reference mortar. Increases of about 3% and of 6 % for M10RP and M20RP were observed compared to the reference mortar. Such observation can be explained by the high porosity of RP and by their high absorption rate [56]. For mortars incorporating LF, the total porosity values are 17.80% and 18.5% for

M10LF and M20LF, respectively. These values represent an increase of 1.5% and of 5% compared to the MR. The substitution of cement paste by some mineral additives is known to increase the total porosity of mortar at early age [57].

At 28 and 90 days, it was observed that mixtures prepared with 10 % RP or LF exhibited similar values of total porosity with an increase of about 2 to 3 % compared to the reference mortar. Meanwhile, compared to the reference mortar, the increase in the total porosity for mixtures prepared with 20 % RP or LF, ranges between 6.6% and 5.6% for M20RP and between 8.8 % and 6.9% for M20LF. Overall, for the same level of replacement of clinker, the mortars formulated with RP or LF have similar water porosities, despite RP being more porous than LF.

The total porosity of mixtures prepared with additives is higher than the reference mortar, mainly due to : 1) the dilution effect, as previously demonstrated and 2) the different reactivity and absorption capacities of RP or LF used in the mixtures resulting in different effective water-to-binder ratio and eventually water-to-cement ratio (see Eqs. 17 and 18). This influences the total porosity since both the effective water-to-cement ratio and the clinker hydration degree govern the volume fraction of capillary pores and hydrates which contain gel pores (see Eqs. 15 and 16).

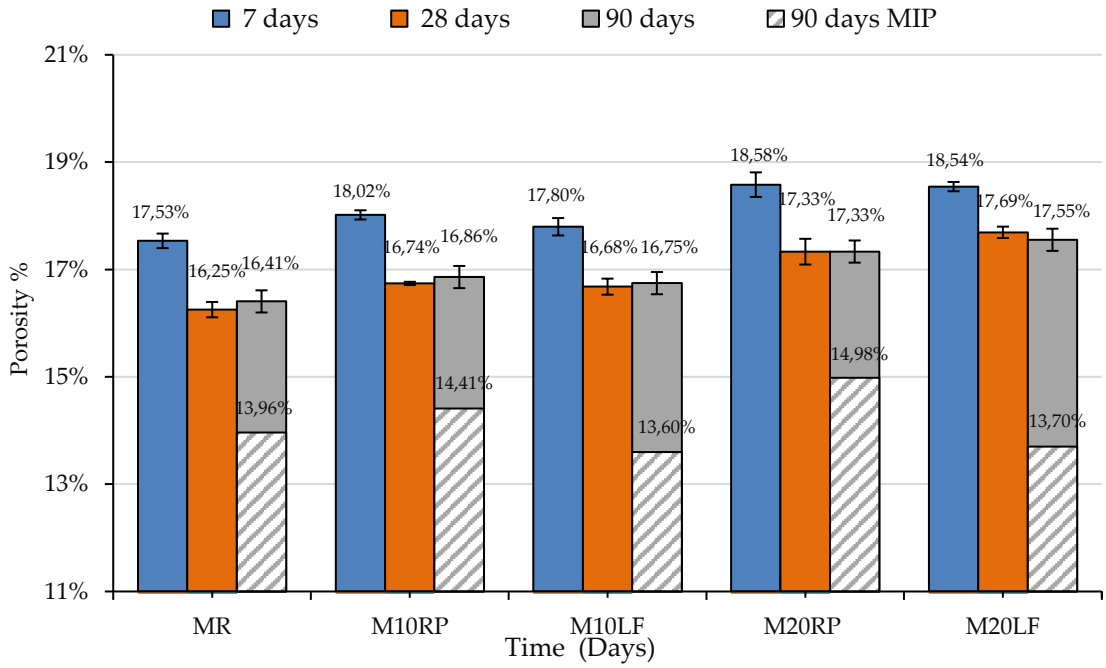

Fig. 8: Water accessible porosity for the reference mortar and mortars with recycled powder and limestone filler at 7, 28 and 90 days. Hashed area: mercury intrusion porosity at 90 days (from one sample per formulation)

4.2.2. Mercury intrusion porosimetry (MIP)

MIP was measured at 90 days for the reference mortar and those formulated with recycled powder and limestone filler at replacement levels of 10 and 20%. The maximum mercury intrusion porosity values at 90 days are presented in Fig. 8. MIP values are smaller than those obtained by water porosity since MIP investigates only pores larger than 6 nm. In contrast to water porosity values, the mixtures containing M10RP and M20RP show higher mercury accessible porosity than MR and mortars prepared with LF.

Fig. 9 a and b show the cumulative pore volume and the differential intrusion as function of pore diameter. The pore size distribution can be classified into three ranges of pore sizes: 1/ Micropores (d<10nm) noted as (Mi), 2/ Mesopores (10nm<d<100nm) noted as (Me), and 3/ Macropores (d>100nm) noted as (Ma) [58]. The pore size distribution is almost similar for all mixtures and concentrated in the second range

Me. For the mixtures containing RP or LF, the maximum concentration of pores is located at 77 nm with an intensity ranged from 0.14 ml/g to 0.18 ml/g. Meanwhile, for MR, two porous modes are observed: a first one located in the Me zone and a second one located in the Ma zone. The cumulative pore volume of M10RP and M20RP was found to be higher than that of other mixtures. It means that the replacement of cement by recycled fines aggregate increases the pore connectivity in the mortar. This result can be explained by the high absorption rate of RP [56], [59] as mentioned previously. The increases in porosity contributes to the decrease in mechanical properties of mortar as discussed in section 4.3. Concerning mortars prepared with LF (M10LF and M20LF), a similar cumulative pore volume was exhibited by both mixtures with a total pore volume value of about 0.063 ml/g.

Fig. 10 shows the pore volume fractions for MR, M10RP, M10LF, M20RP and M20LF. It appears from this figure that the mesopores range is the dominant fraction for all mixtures. The volume fractions of the mesopores is found in the range of 59-67% of the total pore volume. Meanwhile, the volume fractions of the macropores is found in the range of 31-37 % of the total pore volume. Compared to the pore volume fractions of MR, a decrease in the mesopores pore volume fraction an increase in the macropores one was observed for M10RP, M10LF and M20RP. For M20LF, there was no significant change in the volume fractions Me and Ma as compared to MR.

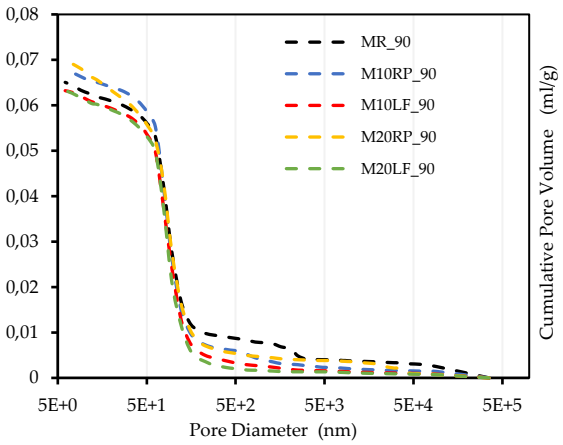

Fig. 9 a: Cumulative pore volume for mixtures at 90 days

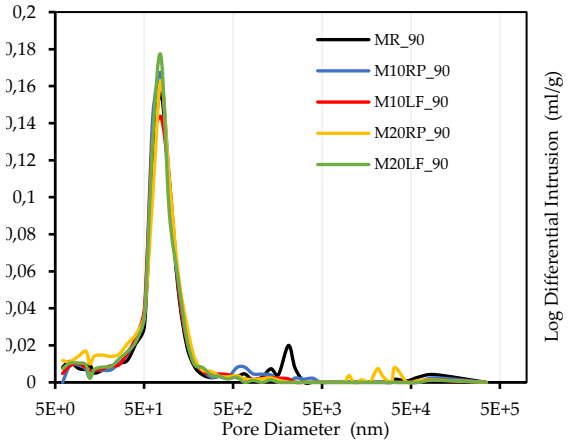

Fig. 9 b: Differential intrusion for mixtures at 90 days

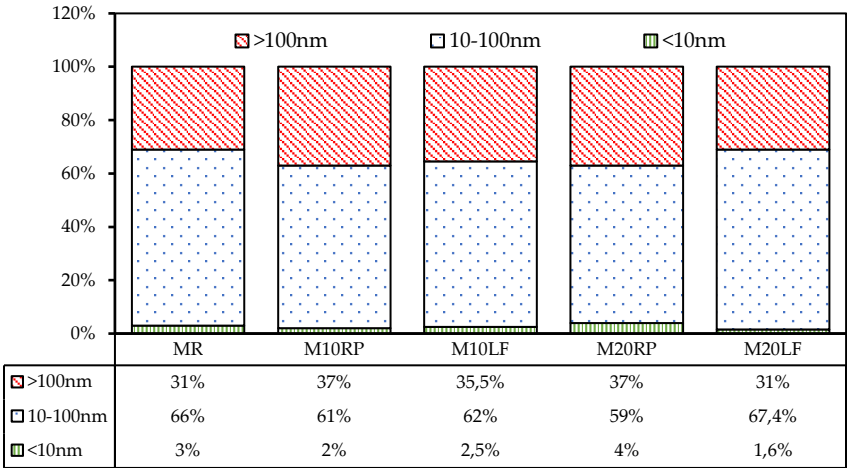

	MR	M10RP	M10LF	M20RP	M20LF
>100nm	31%	37%	35,5%	37%	31%
10-100nm	66%	61%	62%	59%	67,4%
<10nm	3%	2%	2,5%	4%	1,6%

Fig. 10 : Pore-volume fractions for the mortar mixtures at 90 days.

4.2.3. Gas permeability

The gas permeability of the different mortars was measured on three cylinders samples of 70 mm diameter of and 50 mm thickness, at 28 and 90 days. Fig. 11 provides the apparent permeability for mortar mixtures tested (MR, M10RP, M10LF, M20RP and M20LF), which is found to decrease with time. Results presented in Fig. 12 shows the mean of the intrinsic permeability measured on three samples. The evolution of the intrinsic permeability with time is found decreasing or increasing depending on mixtures. Overall, the substitution of clinker by 10 or 20% of RP or LF did not significantly affect permeability.

A decrease in the intrinsic permeability values with time was observed for mortars made with 10 and 20% LF and for MR. Compared to the intrinsic permeability of MR, the intrinsic permeability of M10LF and M20LF is lowered by 17 and 24% at 28 days and by 11 and 8 % at 90 days. The decrease of permeability with time might be due to the continuation of the hydration process which induces the progressive filling of large pores by produced hydrates and on the other hand, to the reduction of connectivity between pores [55], [57].

Unlike mortars prepared with LF, RP-based mortars (M10RP and M20RP) exhibited an increase in the intrinsic permeability between 28 and 90 days. The intrinsic permeability for M10RP increased from 1.21×10^{-17} m^2 to 1.40×10^{-17} m^2 between 28 and 90 days. Similarly, the intrinsic permeability for M20RP increased from 1.45×10^{-17} m^2 to 1.81×10^{-17} m^2 between 28 and 90 days. The moderate increase in the intrinsic permeability for mortars prepared with RP as compared to MR can be explained through the pore size distribution and the interconnection between them as mentioned in the Sec. 4.2.2

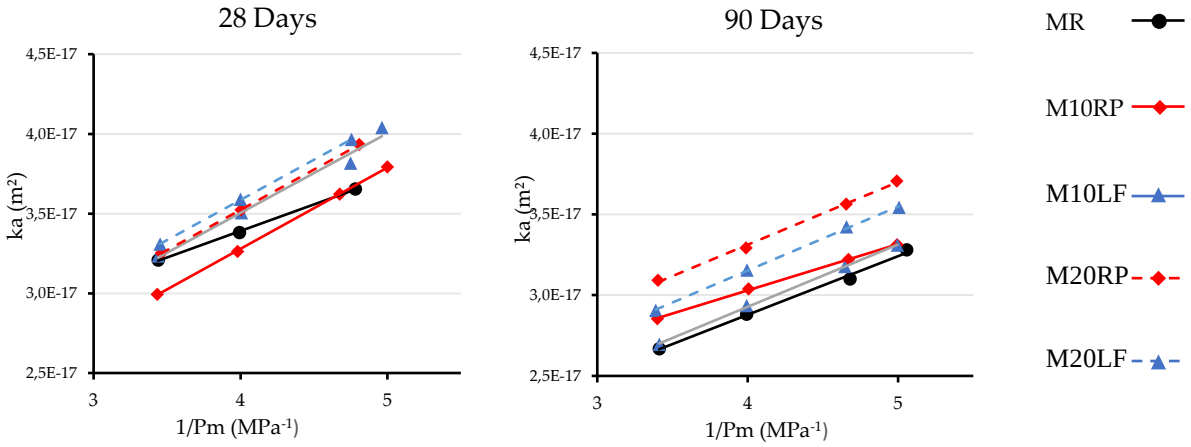

Fig. 11 :Apparent permeability for the reference mortar and mortars with recycled powder and limestone filler at 28 and 90 days.

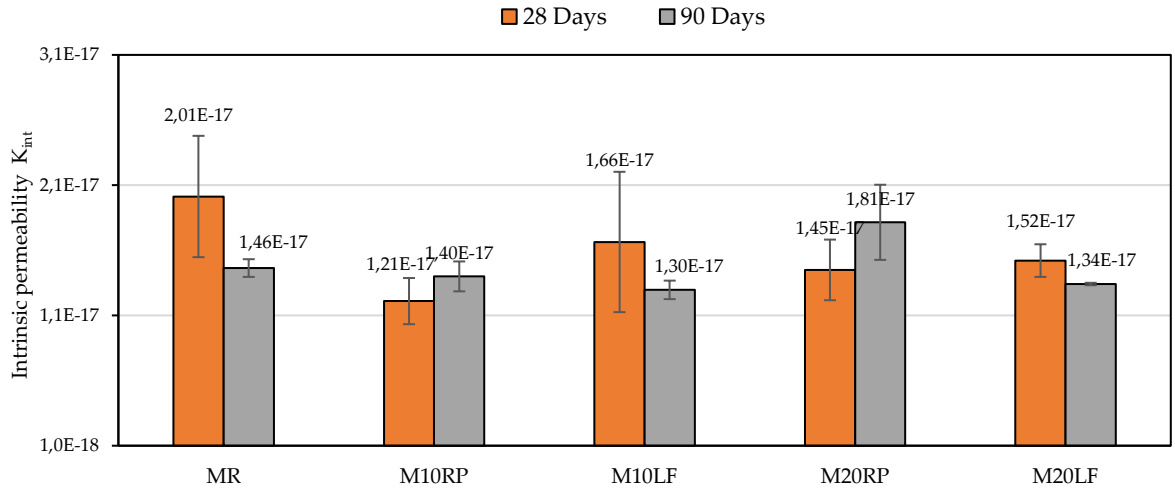

Fig. 12 : Intrinsic permeability for the reference mortar and mortars with recycled powder and limestone filler at 28 and 90 days.

4.3. Mechanical properties

Fig. 13 and Fig. 14 show the results of the compressive strengths and the dynamic modulus evolution for the reference mortar and mortars prepared with RP or LF at 3, 7, 28 and 90 days. It can be clearly seen from these figures that, at all testing age, the mechanical properties of mixtures based on RP or LF have decreased compared to the reference mortar MR, whatever the replacement levels. These results are consistent with hydration degree and porosity results (see section 4.1.3). The decrease in compressive strength for mortars prepared with RP or LF is due directly to the dilution effects [51], [53] and ultimately to the increase in porosity.

The compressive strength of the reference mortar was 37.4, 43.9, 49.6 and 59.2 MPa at 3, 7, 28 and 90 days, respectively. At early ages, samples prepared with 10 % RP of cement replacement caused a decrease in compressive strength by respectively 16 and 20 % for 3 and 7 days. Similarly, samples prepared with 10 % LF of cement replacement caused a decrease in compressive strength by respectively 14 % and 16 % for 3 and 7 days. Mortars prepared with RP in short terms exhibited a lower compressive strength than that of mortars prepared with LF. This might be due to the particle diameter of LF (d_{90} = 35.44 µm) which is smaller than that of RP (d_{90} = 47.14 µm), which means that LF particles may fill more voids of cement matrix compared to the particles (Table 1). Additionally, LF particles are likely more resistant than RP ones. At 28 days, the use of 10 and 20 % RP as cement replacement caused a decrease in the compressive strength by respectively 11 and 18%. For mortars prepared with LF, the decrease in the compressive strength are in the order of 15 and 19%. At 90 days, the reference mortar exhibited a higher compressive strength (59.2 MPa) compared to the compressive strength of mortars prepared with RP or LF. Mortars prepared with RP or LF provided a similar compressive strength (~50 MPa at 10% replacement, ~45-46 MPa at 20% replacement).

Fig. 14 shows the dynamic Young's modulus values of tested mortars at 3, 7, 28 and 90 days. At 3 days and compared to MR, the decrease in modulus was different from one mixture to the other. For samples prepared with RP, the decrease is in the order of respectively 14 and 18% for M10PR and M20PR. However, for mortars samples prepared with LF, the decrease is by about respectively 10 and 11% for 10% M10LF and M20LF. This can be explained by the filler effect of LF at early age. For the other testing ages, the dynamic Young's modulus is almost the same for the mixtures prepared with RP or LF.

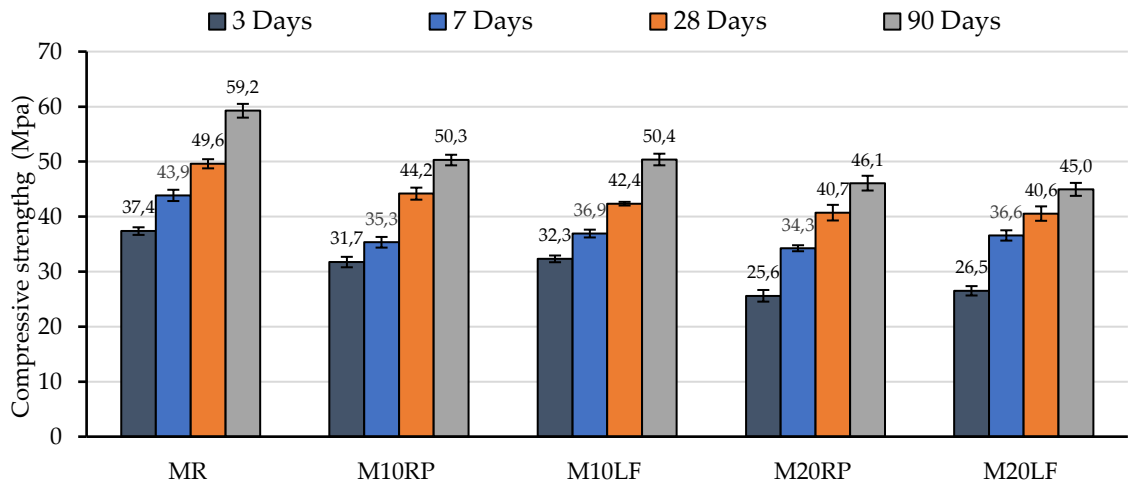

Fig. 13 : Compressive strengths for reference mortar and mortars with recycled powder and limestone filler.

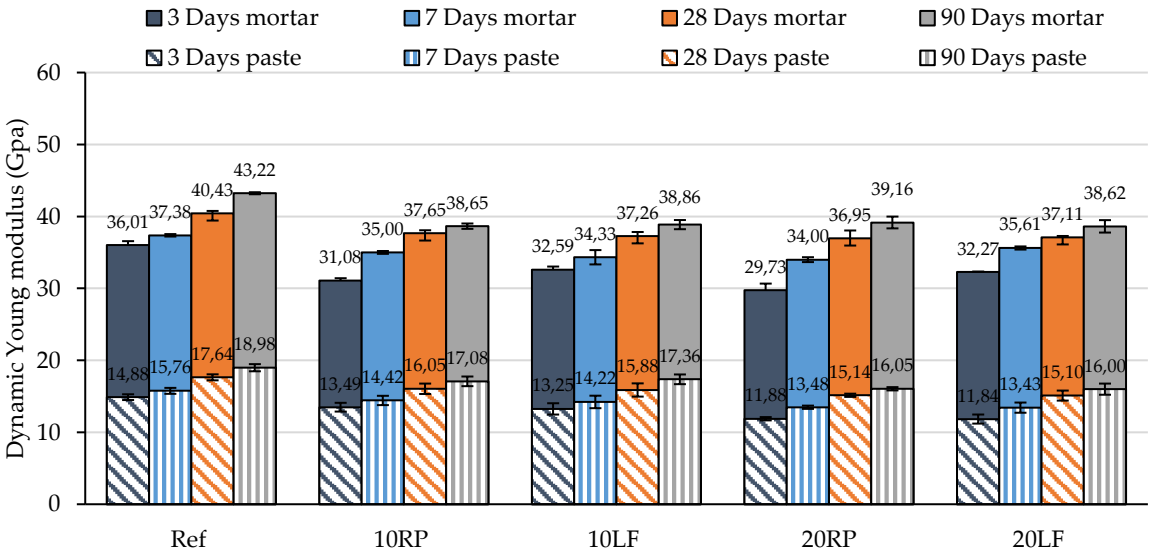

Fig. 14 :Evolution of dynamic modulus for the mortars and cement pastes over time.

In order to gain insights from the multi-scale model, the experimental results on the hydration degree (Fig. 7) and the Young's modulus (Fig. 14) are gathered in Fig. 15 and Fig. 16 to study the evolution of the stiffness along hydration. Results of the multi-scale micromechanical model are also presented. In Fig. 16, results are expressed as a function of the overall hydration degree of the binder, which directly corresponds to values obtained from equation (1) and the experimental TGA values on pastes by the method proposed by Deboucha et al [24]. In Fig. 15, results are expressed as a function of the hydration degree of the clinker only, assuming that additions do not significantly react with clinker, i.e. $\alpha_{binder} = (1 - X)\, \alpha_{clinker}$.

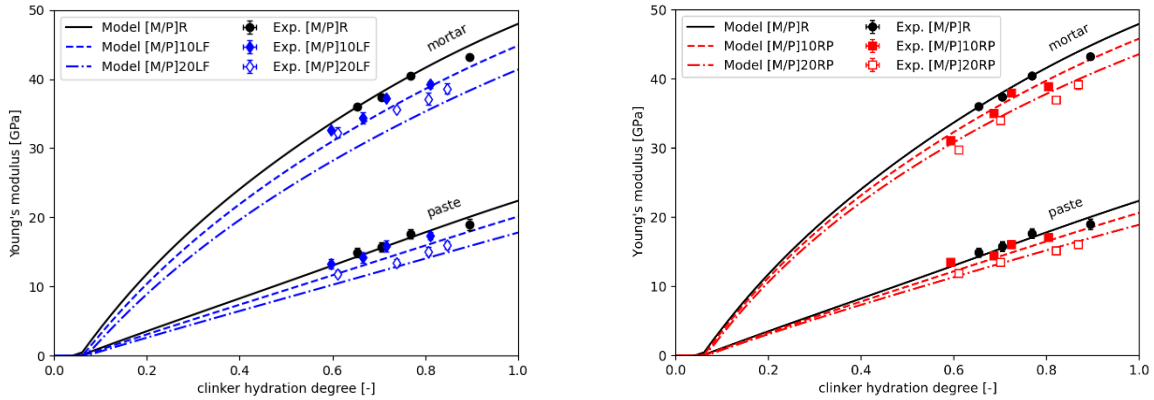

Fig. 15 : Young's modulus in cement pastes and mortars as a function of the hydration degree of clinker, estimated by the multiscale model and experimental values at 3, 7, 28 and 90 days.

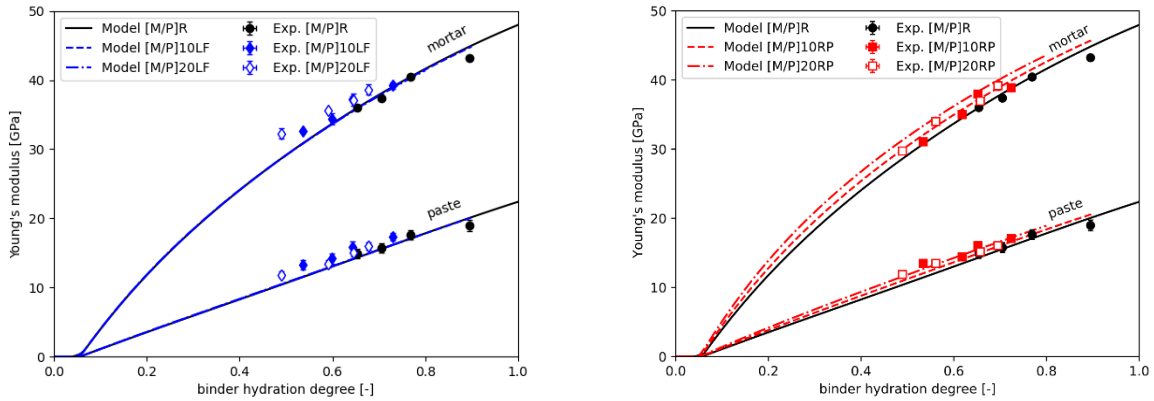

Fig. 16 : Young's modulus in cement pastes and mortars as a function of the overall hydration degree of binder, estimated by the multiscale model and experimental values at 3, 7, 28 and 90 days**.**

The multiscale micromechanical model is in remarkable agreement with experimental results, for all formulations of both pastes and mortars. The assumptions of the model presented in Section 3 provide a possible way to explain the effect of both hydration and substitution of clinker by up to 20% of either LF or RP. Specifically, the reduction in stiffness caused by substitution is mainly attributed to the dilution effect which reduces the overall hydration degree of the binder, or equivalently, increases the effective water-to-cement ratio w/c_{eff} (see equation 17). Further, despite the mechanical properties of RP are much worse than those of LF, cements paste and mortars formulated with RP have elastic moduli similar to those of LF for the same substitution rates. This is accounted for in the multiscale model by the reduction of effective water-to-binder ratio w/b_{eff} (see equation 18), since part of the mix water is adsorbed and reacts with RP. Of course, this beneficial effect comes at the price of a reduced workability. Further, if the reduction of w/c_{eff} is here beneficial for mixtures formulated with a rather elevated initial water-to-binder ratio ($w/b = 0.5$), it may raise workability problems for mixtures with low initial w/b ratios.

5. Conclusions

In this article, experimental investigations and multi-scale modeling of hydration, mechanical and transfer properties of blended cement pastes and mortars prepared with recycled powder or limestone filler are presented. The aim is to provide a better understanding of the contribution of recycled powder to the hydration kinetics as well as transfer and mechanical properties.

Based on the results obtained and the observations made during the experimental tests using different techniques, the following conclusions may be drawn:

- *Hydration:* The replacement of clinker by recycled powder (RP) or limestone filler (LF), leads to generate lower heat of hydration by a dilution effect. The kinetics of hydration of cement paste containing RP or LF is similar.
- *Transfer properties:* At early ages, mortars incorporating RP exhibited a higher total porosity than the reference mortar and mortars prepared with LF. However, at advanced ages, mortars with RP or LF have comparable total porosity. The replacement of clinker by 10-20% of RP slightly increases the fraction of macropores found by MIP and the gas permeability of mortars.
- *Mechanical properties:* The use of RP decreases as much as that of LF the compressive strength and dynamic elastic modulus at early and later ages due to the dilution effect. The replacement of clinker by 10-20% of RP results in a 15-20% reduction in the compressive strength of mortar at 90 days.

Further, the decrease in Young's modulus with partial replacement of clinker by RP or LF is explained and quantitatively reproduced by a multiscale micromechanical model. This decrease is accounted mainly via the modification of the effective water to binder ratio. Despite RP having lower moduli than LF, they lead to comparable mortar moduli due to the reduction of effective water to binder ratio by both absorption in RP porosity and consumption by reaction of residual clinker in RP.

Table 10 summarizes the finding obtained in the present study, which investigated the effect of partial replacement of cement by recycled powder or limestone filler on mechanical properties, hydration degree and transfer properties in cement pastes and mortars.

Table 10*:* Summary table of the results for mixtures incorporating RP or LF (10% ; 20%) compared of the reference at 28 and 90 days.

Material Properties	RP blended paste/mortar				LF blended paste/mortar			
	28 days		90 days		28 days		90 days	
	10 %	20 %	10 %	20 %	10 %	20 %	10 %	20 %
Compressive strength (MPa)	44.2 ▼	; 40.7 ▼	50.3 ▼	; 46.1 ▼	42.4 ▼	; 40.6 ▼	50.4 ▼	; 45 ▼
Young Modul's (MPa)	37.65 ▼	; 36.95 ▼	38.65 ▼	; 39.16 ▼	37.26 ▼	; 37.11 ▼	38.86 ▼	; 38.62 ▼
Degree hydration (%)	65 ▼	; 65 ▼	72 ▼	; 69 ▼	64 ▼	; 64 ▼	73 ▼	; 67 ▼
Water Porosity (%)	16.7 ▲	; 17.3 ▲	16.8 ▲	; 17.5 ▲	16.7 ▲	; 17.7 ▲	16.7 ▲	; 17.5 ▲
Porosity MIP (%)		/	14.4 ▲	; 15 ▲		/	13.6 ▼	; 13.7 ▼
Intrinsic permeability (E-17)	1.21 ▼	; 1.45 ▼	1.4 ▼	; 1.81 ▲	1.66 ▼	; 1.52 ▼	1.30 ▼	; 1.34 ▼

▼: a decrease in the property investigated; ▲: an increase in the property investigated.

Given the variability in the composition and characteristics of demolition waste aggregates obtained from one platform to another, further research is needed to study the influence of these variations; in essence, the intention is to give a general overview on the impact of recycled fine aggregates on concrete properties.

Acknowledgements

Financial support was partly provided by a French-Algerian cooperation project Tassili 19MDU216.

References

[1] J. J. Assaad et M. Vachon, « Valorizing the use of recycled fine aggregates in masonry cement production », *Constr. Build. Mater.*, vol. 310, p. 125263, déc. 2021, doi: 10.1016/j.conbuildmat.2021.125263.

[2] Y. Meng, T.-C. Ling, et K. H. Mo, « Recycling of wastes for value-added applications in concrete blocks: An overview », *Resour. Conserv. Recycl.*, vol. 138, p. 298-312, nov. 2018, doi: 10.1016/j.resconrec.2018.07.029.

[3] J. Pacheco, J. de Brito, C. Chastre, et L. Evangelista, « Experimental investigation on the variability of the main mechanical properties of concrete produced with coarse recycled concrete aggregates », *Constr. Build. Mater.*, vol. 201, p. 110-120, mars 2019, doi: 10.1016/j.conbuildmat.2018.12.200.

[4] C. Thomas, J. de Brito, A. Cimentada, et J. A. Sainz-Aja, « Macro- and micro- properties of multi-recycled aggregate concrete », *J. Clean. Prod.*, vol. 245, p. 118843, févr. 2020, doi: 10.1016/j.jclepro.2019.118843.

[5] T. Ozbakkaloglu, A. Gholampour, et T. Xie, « Mechanical and durability properties of recycled aggregate concrete: effect of recycled aggregate properties and content », *J. Mater. Civ. Eng.*, vol. 30, nº 2, p. 04017275, 2018.

[6] AFNOR, « NF EN 206/CN :Béton -Spécification, performance, production et conformité-Complément national à la norme NF EN 206 ». 2014. Consulté le: 18 juin 2022. [En ligne]. Disponible sur: https://viewerbdc.afnor.org/pdf/viewer/eLn4MkHZB181

[7] C. A. Hendriks, E. Worrell, D. De Jager, K. Blok, et P. Riemer, « Emission reduction of greenhouse gases from the cement industry », in *Proceedings of the fourth international conference on greenhouse gas control technologies*, IEA GHG R&D Programme Interlaken, Austria, 1998, p. 939-944.

[8] T. R. Naik et G. Moriconi, « Environmental-friendly durable concrete made with recycled materials for sustainable concrete construction », in *International Symposium on Sustainable Development of Cement, Concrete and Concrete Structures, Toronto, Ontario, October*, 2005.

[9] R. Kajaste et M. Hurme, « Cement industry greenhouse gas emissions–management options and abatement cost », *J. Clean. Prod.*, vol. 112, p. 4041-4052, 2016.

[10] M.-Y. Xuan, Y. Han, et X.-Y. Wang, « The Hydration, Mechanical, Autogenous Shrinkage, Durability, and Sustainability Properties of Cement–Limestone–Slag Ternary Composites », *Sustainability*, vol. 13, nº 4, Art. nº 4, janv. 2021, doi: 10.3390/su13041881.

[11] Y. Du, W. Yang, Y. Ge, S. Wang, et P. Liu, « Thermal conductivity of cement paste containing waste glass powder, metakaolin and limestone filler as supplementary cementitious material », *J. Clean. Prod.*, vol. 287, p. 125018, mars 2021, doi: 10.1016/j.jclepro.2020.125018.

[12] Y. Li, J. Fang, L. Cheng, X. He, Y. Su, et H. Tan, « Mechanical performance, hydration characteristics and microstructures of high volume blast furnace ferronickel slag cement mortar by wet grinding activation », *Constr. Build. Mater.*, vol. 320, p. 126148, févr. 2022, doi: 10.1016/j.conbuildmat.2021.126148.

[13] D. Wang, C. Shi, N. Farzadnia, Z. Shi, H. Jia, et Z. Ou, « A review on use of limestone powder in cement-based materials: Mechanism, hydration and microstructures », *Constr. Build. Mater.*, vol. 181, p. 659-672, août 2018, doi: 10.1016/j.conbuildmat.2018.06.075.

[14] D. K. Panesar et R. Zhang, « Performance comparison of cement replacing materials in concrete: Limestone fillers and supplementary cementing materials – A review », *Constr. Build. Mater.*, vol. 251, p. 118866, août 2020, doi: 10.1016/j.conbuildmat.2020.118866.

[15] A. M. Rashad, « Effect of limestone powder on the properties of alkali-activated materials – A critical overview », *Constr. Build. Mater.*, vol. 356, p. 129188, nov. 2022, doi: 10.1016/j.conbuildmat.2022.129188.

[16] J. Xiao, Z. Ma, T. Sui, A. Akbarnezhad, et Z. Duan, « Mechanical properties of concrete mixed with recycled powder produced from construction and demolition waste », *J. Clean. Prod.*, vol. 188, p. 720-731, juill. 2018, doi: 10.1016/j.jclepro.2018.03.277.

[17] Z. Duan, S. Hou, J. Xiao, et B. Li, « Study on the essential properties of recycled powders from construction and demolition waste », *J. Clean. Prod.*, vol. 253, p. 119865, avr. 2020, doi: 10.1016/j.jclepro.2019.119865.

[18] A. Barbudo, F. Agrela, J. Ayuso, J. R. Jiménez, et C. S. Poon, « Statistical analysis of recycled aggregates derived from different sources for sub-base applications », *Constr. Build. Mater.*, vol. 28, n° 1, Art. n° 1, mars 2012, doi: 10.1016/j.conbuildmat.2011.07.035.

[19] B. Lu, C. Shi, J. Zhang, et J. Wang, « Effects of carbonated hardened cement paste powder on hydration and microstructure of Portland cement », *Constr. Build. Mater.*, vol. 186, p. 699-708, oct. 2018, doi: 10.1016/j.conbuildmat.2018.07.159.

[20] T. Zhang, M. Chen, Y. Wang, et M. Zhang, « Roles of carbonated recycled fines and aggregates in hydration, microstructure and mechanical properties of concrete: A critical review », *Cem. Concr. Compos.*, vol. 138, p. 104994, avr. 2023, doi: 10.1016/j.cemconcomp.2023.104994.

[21] H. Wu, C. Liang, J. Xiao, J. Xu, et Z. Ma, « Early-age behavior and mechanical properties of cement-based materials with various types and fineness of recycled powder », *Struct. Concr.*, vol. 23, n° 2, p. 1253-1272, 2022, doi: 10.1002/suco.202000834.

[22] Q. Liu, B. Li, J. Xiao, et A. Singh, « Utilization potential of aerated concrete block powder and clay brick powder from C&D waste », *Constr. Build. Mater.*, vol. 238, p. 117721, mars 2020, doi: 10.1016/j.conbuildmat.2019.117721.

[23] Z. Duan, S. Hou, J. Xiao, et A. Singh, « Rheological properties of mortar containing recycled powders from construction and demolition wastes », *Constr. Build. Mater.*, vol. 237, p. 117622, mars 2020, doi: 10.1016/j.conbuildmat.2019.117622.

[24] W. Deboucha, N. Leklou, A. Khelidj, et M. N. Oudjit, « Hydration development of mineral additives blended cement using thermogravimetric analysis (TGA): Methodology of calculating the degree of hydration », *Constr. Build. Mater.*, vol. 146, p. 687-701, août 2017, doi: 10.1016/j.conbuildmat.2017.04.132.

[25] EN NF 197-1, « 197-1. Cement–Part 1: Composition, specifications and conformity criteria for common cements », *Br. Stand. Inst.*, 2000.

[26] N. AFNOR, « NF EN 196-1 Méthodes d'essais des ciments-Partie1: détermination des résistances », 2016.

[27] N. EN, « NF EN 196-3 Méthodes d'essais des ciments Partie 3 Détermination du temps de prise et de la stabilité. », 2017.

[28] W. Deboucha, N. Leklou, et A. Khelidj, « Combination effect of limestone filler and slag on hydration reactions in ternary cements », *Eur. J. Environ. Civ. Eng.*, vol. 0, nº 0, p. 1-16, sept. 2020, doi: 10.1080/19648189.2020.1825233.

[29] W. Deboucha *et al.*, « Reactivity Effect of Calcium Carbonate on the Formation of Carboaluminate Phases in Ground Granulated Blast Furnace Slag Blended Cements », *Sustainability*, vol. 13, p. 6504, juin 2021, doi: 10.3390/su13116504.

[30] P. Mounanga, « Experimental study of the behavior of cement pastes at very young age: Hydration, shrinkage, thermophysical properties », *Adv Cem Res*, vol. 16, p. 95-103, 2003.

[31] P. NF, « NF P 18-508. Additions for concrete-Limestone Additions-Specifications and conformity criteria. », 2012.

[32] A. ASTM, « ASTM E 1876-01: standard test method for dynamic young's modulus, shear modulus, and poisson's ratio by impulse excitation of vibration », *Annu. Book ASTM Stand. ASTM West Conshohocken*, 2015.

[33] E. NF, « NF EN ISO 12680-1. Methods of test for refractory products-Part 1 : Determination of dynamic Young's modulus (MOE) by impulse excitation of vibration », 2007.

[34] P. AFNOR, « NF P 18-459 Concrete–Testing hardened concrete–Testing porosity and density », 2010.

[35] P. national GranDuBé (France), *GranDuBé: grandeurs associées à la durabilité des bétons*. Presses de l'École nationale des ponts et chaussées, 2007.

[36] ISO, « ISO 15901-1 Evaluation of pore size distribution and porosity of solid materials by mercury porosimetry and gas adsorption-Part 1 :Mercury porosimetry », 2016.

[37] A. Zaoui, « Continuum micromechanics: survey », *J. Eng. Mech.*, vol. 128, nº 8, p. 808-816, 2002.

[38] L. Dormieux, D. Kondo, et F.-J. Ulm, *Microporomechanics*. John Wiley & Sons, 2006.

[39] M. Kachanov et I. Sevostianov, *Micromechanics of materials, with applications*, vol. 249. Springer, 2018.

[40] J. D. Eshelby, « The determination of the elastic field of an ellipsoidal inclusion, and related problems », *Proc. R. Soc. Lond. Ser. Math. Phys. Sci.*, vol. 241, nº 1226, p. 376-396, 1957.

[41] M. Achour, F. Bignonnet, J.-F. Barthélémy, E. Rozière, et O. Amiri, « Multi-scale modeling of the chloride diffusivity and the elasticity of Portland cement paste », *Constr. Build. Mater.*, vol. 234, p. 117124, févr. 2020, doi: 10.1016/j.conbuildmat.2019.117124.

[42] T. Mori et K. Tanaka, « Average stress in matrix and average elastic energy of materials with misfitting inclusions », *Acta Metall.*, vol. 21, nº 5, p. 571-574, mai 1973, doi: 10.1016/0001-6160(73)90064-3.

[43] Y. Benveniste, « A new approach to the application of Mori-Tanaka's theory in composite materials », *Mech. Mater.*, vol. 6, nº 2, p. 147-157, juin 1987, doi: 10.1016/0167-6636(87)90005-6.

[44] R. J. Hill, « A self-consistent mechanics of composite materials », *J. Mech. Phys. Solids*, vol. 13, nº 4, p. 213-222, 1965, doi: 10.1016/0022-5096(65)90010-4.

[45] B. Pichler et C. Hellmich, « Upscaling quasi-brittle strength of cement paste and mortar: A multi-scale engineering mechanics model », *Cem. Concr. Res.*, vol. 41, nº 5, p. 467-476, mai 2011, doi: 10.1016/j.cemconres.2011.01.010.

[46] T. C. Powers et T. L. Brownyard, « Studies of the Physical Properties of Hardened Portland Cement Paste », *J. Proc.*, vol. 43, nº 9, p. 101-132, sept. 1946, doi: 10.14359/8745.

[47] O. Bernard, F.-J. Ulm, et E. Lemarchand, « A multiscale micromechanics-hydration model for the early-age elastic properties of cement-based materials », *Cem. Concr. Res.*, vol. 33, nº 9, Art. nº 9, sept. 2003, doi: 10.1016/S0008-8846(03)00039-5.

[48] P. Acker, « Micromechanical analysis of creep and shrinkage mechanisms », *Creep Shrinkage Durab. Mech. Concr. Quasi-Brittle Mater. Camb. MA*, p. 15-25, 2001.

[49] M. Zajac et M. Ben Haha, « Experimental investigation and modeling of hydration and performance evolution of fly ash cement », *Mater. Struct.*, vol. 47, nº 7, Art. nº 7, juill. 2014, doi: 10.1617/s11527-013-0126-1.

[50] T. J. Ahrens, *Mineral Physics & Crystallography: A Handbook of Physical Constants*, vol. 2. Washington, DC: American Geophysical Union, 1995. Consulté le: 13 octobre 2022. [En ligne]. Disponible sur: https://resolver.caltech.edu/CaltechAUTHORS:20181127-140646856

[51] M. Cyr, P. Lawrence, et E. Ringot, « Efficiency of mineral admixtures in mortars: Quantification of the physical and chemical effects of fine admixtures in relation with compressive strength - ScienceDirect », 2006. https://www.sciencedirect.com/science/article/pii/S0008884605001687?via%3Dihub#section.0030 (consulté le 17 juin 2022).

[52] P. Mounanga, M. Bouasker, A. Pertue, A. Perronnet, et A. Khelidj, « Early-age autogenous cracking of cementitious matrices: physico-chemical analysis and micro/macro investigations », *Mater. Struct.*, vol. 44, nº 4, p. 749-772, mai 2011, doi: 10.1617/s11527-010-9663-z.

[53] M. Aqel et D. K. Panesar, « Hydration kinetics and compressive strength of steam-cured cement pastes and mortars containing limestone filler », *Constr. Build. Mater.*, vol. 113, p. 359-368, juin 2016, doi: 10.1016/j.conbuildmat.2016.03.031.

[54] B. Lothenbach, G. Le Saout, E. Gallucci, et K. Scrivener, « Influence of limestone on the hydration of Portland cements », *Cem. Concr. Res.*, vol. 38, nº 6, p. 848-860, juin 2008, doi: 10.1016/j.cemconres.2008.01.002.

[55] Y.-X. Li, Y.-M. Chen, J.-X. Wei, X.-Y. He, H.-T. Zhang, et W.-S. Zhang, « A study on the relationship between porosity of the cement paste with mineral additives and compressive strength of mortar based on this paste », *Cem. Concr. Res.*, vol. 36, nº 9, p. 1740-1743, sept. 2006, doi: 10.1016/j.cemconres.2004.07.007.

[56] A. Yammine, N. Leklou, M. Choinska, F. Bignonnet, et J.-M. Mechling, « DEF damage in heat cured mortars made of recycled concrete sand aggregate », *Constr. Build. Mater.*, vol. 252, p. 119059, 2020.

[57] S. P. Pandey et R. L. Sharma, « The influence of mineral additives on the strength and porosity of OPC mortar », *Cem. Concr. Res.*, vol. 30, nº 1, p. 19-23, janv. 2000, doi: 10.1016/S0008-8846(99)00180-5.

[58] K. Li, Q. Zeng, M. Luo, et X. Pang, « Effect of self-desiccation on the pore structure of paste and mortar incorporating 70% GGBS », *Constr. Build. Mater.*, vol. 51, p. 329-337, janv. 2014, doi: 10.1016/j.conbuildmat.2013.10.063.

[59] A. Yammine, M. Hamdadou, N. Leklou, F. Bignonnet, et M. Choinska-Colombel, « Effect of recycled concrete aggregates and recycled filler on delayed ettringite formation: An experimental study compared to chemical modelling », *Cem. Concr. Compos.*, vol. 132, p. 104636, sept. 2022, doi: 10.1016/j.cemconcomp.2022.104636.